LUNDS UNIVERSITET
Lunds Tekniska Högskola

Modeling and Performance Analysis of Alternative Heat Exchangers for Heavy Vehicles

Wamei Lin

Thesis for the degree of Licentiate of Engineering, 2011

Division of Heat Transfer
Department of Energy Sciences
Faculty of Engineering (LTH)
Lund University

www.energy.lth.se

Division of Heat Transfer
Department of Energy Sciences
Faculty of Engineering
Lund University
Box 118, SE-221 00, Lund, Sweden

ISRN LUTMDN/TMHP -- 11/7076 -- SE
ISSN 0282-1990

Abstract

Cross flow heat exchangers made in aluminum are common as radiators in vehicles. However, due to the increasing power requirement and the limited available space in the vehicles, it is extremely difficult to increase the size of the heat exchangers (HEXs) placed in the front of the vehicles. Placing the heat exchanger at the roof or the underbody of the vehicles might increase the possibility to increase the size of the heat exchangers. A new configuration of the heat exchangers has to be developed to accommodate the position change. In this study, a countercurrent heat exchanger is proposed for the position on the roof of the vehicle compartment. Furthermore, a new material, graphite foam having high thermal conductivity (1700 W/(m·K)) and low density (0.2 to 0.6 g/cm^3), is introduced as a potential material for heat exchangers in vehicles.

In order to find an appropriate configuration of fins with high thermal performance and low pressure loss on the air side for a countercurrent flow HEX, the CFD (computational fluid dynamics) approach is applied for a comparative study among louver fin, wavy fin, and pin fin (made in aluminum) by using the ANSYS FLUENT software. Moreover, the comparison between the corrugated, wavy corrugated, pin-finned, and baffle graphite foam fins are also carried out by the ANSYS FLUENT code. The simulation results are verified by experimental results from literature.

Also, a conventional cross flow HEX (made in aluminum) is compared with countercurrent flow aluminum HEXs (made in aluminum or graphite foam), in terms of the thermal performance and the pressure loss. Furthermore, an overall performance comparison between the cross flow HEX and the countercurrent flow HEX is carried out as well, to investigate the coefficient of performance (COP), power density (PD), and compactness factor (CF). For a specific case, the overall size and weight of the countercurrent flow HEXs are much lower than those of the cross flow HEX. However, due to the high pressure loss in the graphite foam HEX, the air pumping power of the countercurrent flow graphite foam HEX is much higher than that of the cross flow aluminum HEX. Useful recommendations are highlighted to promote the development of countercurrent flow HEXs in vehicles.

Keywords: heat exchanger, vehicle, countercurrent flow, graphite foam, thermal performance, pressure loss, fin, computational fluid dynamics, modeling.

Acknowledgements

This work has been carried out at the Division of Heat Transfer, Department of Energy Sciences at Lund University, Lund, Sweden. This study and associated paper and conference participation are financially supported by the Swedish Energy Agency and industries.

I would like to express my great appreciation to my thesis supervisor, Professor Bengt Sundén, for giving me this wonderful opportunity to pursue my postgraduate study in Sweden. I also thank for his helpful support, guidance, encouragement and kindness over the past two years. Furthermore, I would like to thank my co-supervisor, Professor Jinliang Yuan, for his fruitful support, guidance and discussions throughout this work. Also I thank my another co-supervisor, Professor Lennart Löfdahl (Chalmers University of Technology), for suggestion, guidance and discussions about my PhD studies. Thanks to Lisa Larsson for sharing her knowledge about the fluid dynamics of vehicles.

In addition, I would like to thank Dr. Gongnan Xie for his help in my studies and life in the first year. Also I thank Dr. Lei Wang and Dr. Zhenghua Yan for their support. Also I would like to give my many thanks to my colleagues and my Chinese friends, who gave me a happy environment for my study.

Finally, I would like to thank my parents for guiding me patiently and supporting my choice and study all the time. Thanks to my sisters, brother, and my husband.

List of publications

Publications included in this thesis:

1. **Wamei Lin**, and Bengt Sundén, 2010, "Vehicle Cooling Systems for Reducing Fuel Consumption and Carbon Dioxide: Literature Survey", SAE Technical Paper 2010-01-0157.

2. **Wamei Lin**, and Bengt Sundén, 2010, "A Review of Cooling Systems in Electric/Hybrid Vehicles", Proceeding of the ASME 2010 International Mechanical Engineering Congress & Exposition (IMECE2010-37636), November 12-18, 2010, Vancouver, British Columbia, Canada.

3. **Wamei Lin**, and Bengt Sundén, 2011, "Graphite Foam Heat Exchanger for Vehielces", Vehicle Thermal Management Systems Conference & Exhibition 2011, May 15-19, 2011, Heritage Motor Centre, Gaydon, Warwickshire, UK.

4. **Wamei Lin**, Jinliang Yuan, and Bengt Sundén, 2011, "Review on Graphite Foam as Thermal Material for Heat Exchangers", World Renewable Energy Congress 2011, May 8-11, 2011, Linköping, Sweden.

5. **Wamei Lin**, Jinliang Yuan, and Bengt Sundén, 2011, "Performance Analysis and Comparison between Aluminum and Graphite Foam Heat Exchangers under Countercurrent Flow Conditions", 2011 International Workshop on Heat Transfer Advances for Energy Conservation and Pollution Control (IWHT2011-101), October 17-20, 2011, Xi'an, China.

6. **Wamei Lin**, Jinliang Yuan, and Bengt Sundén, 2011, "Performance Analysis of a Countercurrent Flow Heat Exchanger Placed on the Truck Compartment Roof", Proceeding of the ASME 2011 International Mechanical Engineering Congress & Exposition (IMECE2011-62520), November 11-17, 2011, Denver, Colorado, USA.

Publication not included in this thesis:

1. **Wamei Lin**, Jinliang Yuan, and Bengt Sundén, 2010, "Waste Heat Recovery System for Fuel Cell System", International Green Energy Conference (IGEC 2010), June 1-3, 2010, Waterloo, Ontario Canada.

Table of Contents

Nomenclature

A_c	minimum free-flow area [m^2]
A_o	total heat transfer surface area on the air side [m^2]
C	wetted perimeter of the minimum free-flow channel [m]
C_F	Forchheimer coefficient [-]
c_p	specific heat [$J \cdot kg^{-1} \cdot K^{-1}$]
D_h	hydraulic diameter [m]
d_p	pore diameter [m]
f	friction factor [-]
h	heat transfer coefficient [$W \cdot m^{-2} \cdot K^{-1}$]
k	turbulent kinetic energy [$m^2 \cdot s^{-2}$]
m	mass [kg]
Nu	Nusselt number [-]
P	power [W]
Pr	Prandtl number [-]
p	pressure [Pa]
Q	total amount of heat dissipated to air [W]
Re	Reynolds number [-]
St	Stanton number [-]
T	temperature [K]
u, v, w	velocity components in x, y and z directions, respectively [$m \cdot s^{-1}$]
u_i'	fluctuation from the mean velocity u_i [$m \cdot s^{-1}$]
V	volume [m^3]
Δp	pressure drop [Pa]
ΔT	logarithmic mean temperature difference [K]

Greek symbols

α	permeability [m^2]
γ	area to volume ratio [$m^2 \cdot m^{-3}$]
ε	rate of energy dissipation
λ	thermal conductivity [$W \cdot m^{-1} \cdot K^{-1}$]

μ	dynamic viscosity of fluid [Pa·s]
v	kinematic viscosity of fluid [$m^2 \cdot s^{-1}$]
ρ	density [$kg \cdot m^{-3}$]
φ	porosity [-]

Subscripts

air	air
eff	effective
f	fluid
HEX	heat exchanger
in	inlet
i, j	coordinate indices
max	maximum
out	outlet
pump	pump
removed	removed
s	solid
t	turbulence
w	wall
water	water

Abbreviations

Al	aluminum
CAB	controlled atmosphere brazing
CC	countercurrent flow
CF	compactness factor
CO	carbon monoxide
CO_2	carbon dioxide
COP	coefficient of performance
CR	cross flow
FVM	finite volume method
G	graphite foam
H	height
HC	hydrocarbon

HEX	heat exchanger
L	length
LMTD	logarithmic mean temperature difference
ORNL	Oak Ridge National Laboratory
PCM	phase change material
PD	power density
RNG	renormalization group
SIMPLE	Semi-Implicit Method for Pressure Linked Equations
W	width

1 Introduction

The present work is based on a research project "Development of new cooling systems for heavy vehicles - for reduced fuel consumption and lower carbon dioxide emission", which has been financially supported by the Swedish Energy Agency and industries. There are two major parts in this project. One is the flow field analysis around a heavy vehicle, which is carried out by Chalmers University of Technology. The other part is the heat exchanger design for a heavy vehicle, which is implemented by Lund University.

This work is focused on the heat exchanger design for heavy vehicles, which includes modeling, simulation and analysis of heat transfer and fluid flow in a new (countercurrent flow) heat exchanger. The developed models are validated by experimental data from the literature. Based on the simulation results, the heat exchanger should be optimized in terms of thermal performance and flow resistance, which would be provided to Chalmers University of Technology to further optimize the flow field around the heavy vehicles.

1.1 Background

In recent years the number of vehicles being used has constantly increased. For instance, the number of registrated trucks and buses increased from 138 million to 274 million between 1990 and 2008 in the world. The increasing number of vehicles causes more energy/fuel to be consumed and more carbon dioxide (CO_2) to be released to the environment. 29.2 % of the total energy in USA are consumed by the transportation section (medium/heavy trucks used 18.7 % of energy in transportation) in 2008. Furthermore, 31.2 % of CO_2 emission was from the transportation section (67.9 % from medium/heavy trucks and buses) in USA [1]. On the other hand, the oil price is increasing all the time. Strong legislations on emissions have been introduced as well. All these factors require innovations in the vehicle industry.

Many technical developments have been introduced to meet the requirements on low fuel consumption and CO_2 emission in vehicles. Concerning the energy distribution (as shown in Fig. 1.1) in the vehicle, only around 35 % of the total fuel energy finally becomes mechanical work which is used for driving the vehicle. However, 30 % of the total energy input is brought away by the coolant of the engine cooling system, and another 35 % of the energy is lost to the exhaust gases. If one could optimize the energy wasted in the coolant or the exhaust gases, the fuel consumption and the CO_2 emission (this is also proportional to the fuel consumption) could be reduced.

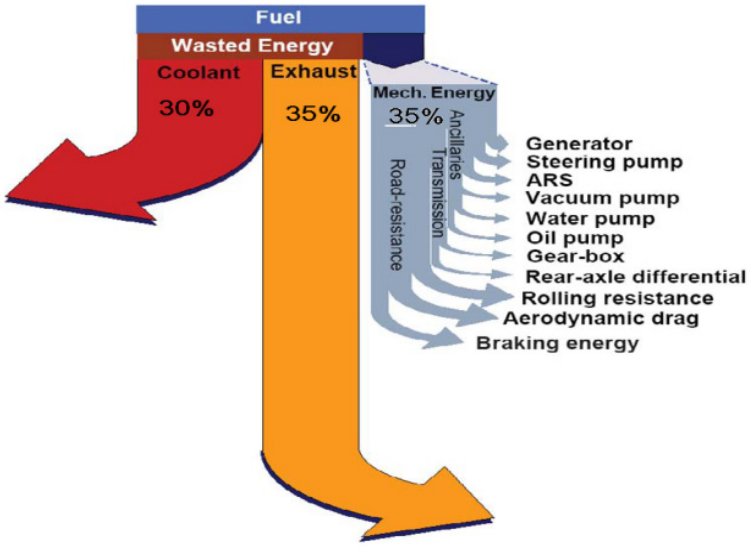

Fig. 1.1. Energy distribution in a vehicle [2].

One third of the engine energy is lost to the exhaust gases. Johnson [3] found out for a typical 3.0 liter gas engine with a maximum mechanical output power of 115 kW, the total waste heat dissipated can be from 20 kW to as much as 400 kW across the range of a typical engine operation. The corresponding energy efficiency of the vehicles might be from 30 % to 15 %. If the exhaust gases enter into the surroundings directly, they will not only waste energy but also cause heat pollution of the environment. Reusing the waste heat of the exhaust gas has a great potential for reducing the fuel consumption of vehicles. There are several methods to reuse the energy of the exhaust gases. These methods include:

(1) The waste heat is used to heat the passenger compartment in the winter;

(2) The waste heat can be used in absorption cooling, which is attractive for the tractor-trailer refrigeration and bus air conditioning systems;

(3) The waste heat from exhaust gases is reused to generate electricity by using a thermoelectric device (3 -8 % fuel saving is offered by a thermoelectric generator [4]).

However, due to development of electric or hybrid electric vehicles and fuel cell vehicles, less and less exhaust gases are dissipated from the vehicles. In this case, more heat has to be brought away by the engine cooling system than before (the engine efficiency is assumed similar). Furthermore, the working temperature of batteries (electric vehicles) is around 55 ℃ [5], and the operating temperature of Polymer Electrolyte Membrane Fuel Cells (used for fuel cell vehicles) is around 65 ℃ [6]. These temperatures of electric vehicles or fuel cell vehicles are much lower than that of a combustion engine vehicle (the working temperature is around 90 ℃). Due to the low working temperature of electric or fuel cell vehicles, the size of the heat exchanger (HEX) has to be increased. However, there is space limitation in vehicles. Thus, the cooling issues become more serious than before.

If the engine cooling system can not bring away the heat quickly, the engine working temperature will increase. More fuel will be consumed and the life time of the engine

will be reduced due to the high working temperature in the engine. Contrarily, a good engine cooling system can reduce the time of the engine start and warm up processes, in which the engine reaches its optimal working temperature [7]. A lot of hydrocarbon (HC) and carbon monoxide (CO) are produced during the starting and warming up period [8]. Thus, an efficient engine cooling system is significantly important for the fuel consumption of vehicles.

1.2 Tasks of the study

The overall aim of this study is to develop a new cooling system to satisfy the increasing cooling power in vehicles. There are two methods for the new cooling system in the vehicle.

1) Changing the position of heat exchangers: Due to the space limitation in vehicles, it is extremely difficult to increase the size of the heat exchangers (HEXs) to bring away the increased heat from the vehicles. Removing the HEX from the front of the vehicles to the roof of vehicles, might increase the possibility to increase the size of the HEX. However, when the HEX is placed at the roof, a new configuration of the HEX has to be introduced to accommodate the HEX position change. Based on the air fluid direction and the engine coolant direction, a countercurrent flow HEX is introduced at the roof position, to replace a cross flow HEX.

2) Using graphite foam as a thermal material for HEXs in vehicles: Nowadays aluminum HEXs are very common in the vehicle industry. Due to the increasing cooling power and the space limitation in vehicles, a highly compact HEX has to be developed. Graphite foam has even higher thermal conductivity (solid thermal conductivity is around 1700 W/m·K), large specific surface area (5000-50000 m^2/m^3), and low density (0.2-0.6 g/cm^3). These characteristics imply that graphite foam is a good potential thermal material for HEXs (instead of the conventional aluminum HEX).

In order to analyze the thermal performance and flow characteristics of the new HEXs in vehicles, numerical calculation methods are developed to compare among different configurations of aluminum HEXs, and different configurations of graphite foam ones. The major tasks in this study are as follows:

I. Four different configurations (corrugated, wavy corrugated, pin-finned, and baffle) of graphite foam HEXs are analyzed, to find out which configuration produces better thermal performance and lower pressure drop.

II. Three different configurations (wavy -, pin - and louver fin) of aluminum HEXs are analyzed in terms of thermal performance and pressure loss.

III. The fin configurations with high thermal performance and low pressure loss are chosen for the aluminum HEXs and graphite foam HEXs, respectively. A comparison between the countercurrent flow HEXs (made in graphite foam or aluminum) and the cross flow aluminum HEX are carried out, to evaluate the coefficient of performance (COP), power density (PD), and compactness factor (CF).

IV. A case study is carried out to compare a cross flow HEX (aluminum) with a countercurrent flow HEX (made in aluminum, or graphite foam), to evaluate the advantages/disadvantages of the countercurrent flow HEXs.

1.3 Methodology

A literature survey is carried out to review the performed research and development work for the engine cooling system, thermal management of vehicles, and the heat exchanger or radiator in the vehicle. Based on the review work, the study will focus on the design of a countercurrent flow HEX made in aluminum or graphite foam.

In order to simplify the simulation model, only a core of the HEX is considered in this work. The symmetry or periodic boundary condition is applied to represent the operating condition of the whole HEX. Furthermore, a finite volume method (FVM) is adopted to convert the governing equations to algebraic equations in the modeling. The Semi-Implicit Method for Pressure Linked Equations (SIMPLE) algorithm is used to couple pressure and velocity, as implemented in the commercial software ANSYS FLUENT. The simulation models are validated by experiment results from the literature.

The thermal performance and the pressure loss are the two important factors in the heat exchanger design. In order to develop a high performance countercurrent flow HEXs, the thermal performance and pressure loss will be analyzed for different configurations of fins (aluminum HEX: louver-, wavy- and pin fin; graphite foam HEX: corrugated, wavy corrugated, pin-finned, and baffle fins) on the air side of a HEX. Flat tubes are used on the water side. Moreover, the coefficient of performance (COP), power density (PD), and compactness factor (CF) will be analyzed for the aluminum HEX and the graphite foam HEX, to evaluate the overall performance of the graphite foam HEX (due to the high pressure drop in graphite foam, a lot of concern is the overall performance of HEXs).

1.4 Outline of thesis

After presenting the introduction of this study in Chapter 1, a literature survey will be outlined in Chapter 2, in which the research work on vehicle cooling systems (including different methods of thermal management in vehicles), thermal performance and flow characteristics of graphite foam are reviewed. Furthermore, the development of heat exchangers in vehicles will be included in Chapter 2. The physical model and numerical methods will be provided in Chapter 3, in which the governing equations, the corresponding boundary conditions, together with solution methods and meshing are presented. The simulation results will be presented in Chapter 4. Meanwhile, the model validation is also carried out in Chapter 4. The conclusion and suggestion based on this study are drawn and highlighted in Chapter 5. Finally, the ideas for the future work will be conceived in Chapter 6.

2 Literature survey

The purpose of this chapter is to review different research and development works on vehicle cooling systems. In the first part of this chapter, basic information about engine cooling systems will be presented. The methods for improving the thermal management of the engine cooling will be reviewed in the second part. In the third part, different methods to increase the thermal performance of heat exchangers/radiators, and manufacturing methods will be summarized.

2.1 Engine cooling systems

There are two major types of engine cooling systems. One is the air cooling system, another is the liquid cooling system. Nowadays the air cooling is only used in older cars or some modern motorcycles. The liquid cooling system plays an important role in the most automobiles. A typical engine cooling system is shown in Fig. 2.1. There are two major heat exchangers:

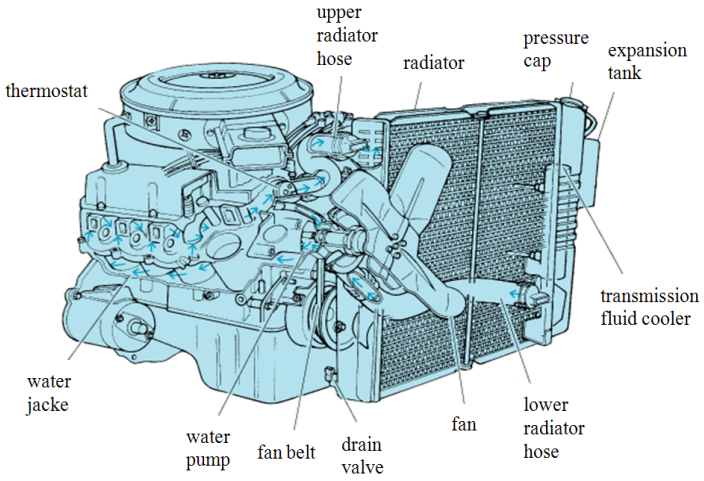

(a)

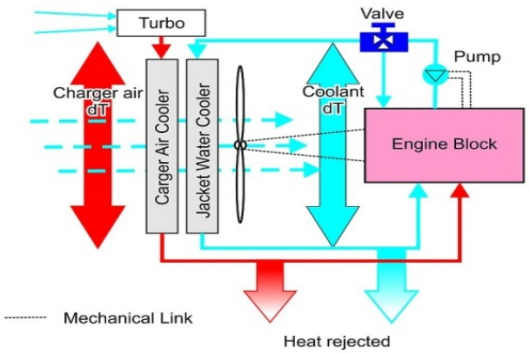

(b)

Fig. 2.1. Engine cooling systems: (a) 3-D model [9]; (b) 2-D model [10].

1) **Engine water jacket cooler (radiator)**: It is significant to operate at an appropriate temperature for better performance of engines. If the engine always works at extremely high temperature, it will not lead to an optimal combustion process, which causes the aging of the lubricant oil and break down of engine material problems. However, if it is cold, the engine will be less efficient and emit more pollution. Thus, there has to be a water jacket around the engine to keep the engine working at an optimal temperature. The engine coolant brings the redundant heat from the engine water jacket to a radiator. Then the radiator dissipates the heat to the ambient. The coolant will return to the water jacket to continue the next cooling cycle.

2) **Charged air cooler (internal cooler)**: Fresh air firstly passes a turbocharger (Turbo) to increase the pressure and increase the density of the air. In this case, more air can enter the engine to achieve a sufficient combustion process. However, after the turbocharger, the temperature of the fresh air is increased as well. The high temperature reduces the density of oxygen in the fresh air. Low content of oxygen leads to an inadequate combustion process. Thus, an internal cooler is introduced to cool the fresh air after the turbocharger to increase the content of oxygen before the air enters the engine.

2.2 Thermal management

A good thermal management of the engine cooling system may extend the life time of both the engine and the components in the engine cooling system. A good thermal management also has an impact on the fuel consumption and CO_2 emissions. Electrification of the cooling fan or pump, using new materials, or rearranging the position of the heat exchangers may significantly improve the thermal management of engine cooling system.

2.2.1 Electrification of cooling system components

In a combustion engine, the engine not only gives power to speed up the vehicle, but also gives power to the cooling fan and the water pump. Thus, the speed of the cooling fan and the water pump is controlled by the engine speed. This method is not efficient for the cooling performance and the fuel consumption in vehicles. If the cooling fan or water pump is controlled by a separate system, then the efficiency of the cooling fan or water pump might be optimized. Staunton et al. [10] analyzed several advanced thermal management system topologies. A thermal management system with an array of small electrical fans was installed instead of a mechanical fan. When the engine cooling system was fully electrified, 17 kW was saved in a micro-hybrid vehicle, and 14.5 kW was saved in a standard diesel vehicle as well. Cho et al. [11] demonstrated that more than 87 % of the pumping power could be saved by using an electric pump instead of a mechanical one. Moreover, the radiator size could also be reduced by more than 27 % as an electric pump was used. Thus, the electrical cooling fan or water pump in the engine cooling system has a great importance in reducing the power consumption in vehicles.

2.2.2 New materials (phase change material, nanofluid)

New material development promotes a good thermal management in vehicles. The nanotechnology might be used to improve the thermal conductivities of the engine coolant, because of the high thermal conductivity in "nanofluids" (due to the high thermal conductivity of nanoparticles and the diffusion of the nanoparticles) [12]. Leong et al. [13] showed that 3.8 % of heat transfer enhancement could be achieved with the addition of 2 % copper particles in an engine coolant. 18.7 % reduction of the air frontal area was achieved as well. However, the pumping power of the coolant was increased by 12.13 %. Furthermore, Kulkarni et al. [14] analyzed nanofluids as coolants in a diesel electric generator. The specific heat of the nanofluids was reduced by increasing the nanoparticle concentration. However, the HEX efficiency was increased with increasing nanoparticle concentration.

Another new material, so-called phase change material (PCM), improves the thermal management of vehicles especially for electric vehicles [15]. The principle of PCM is that the state of the PCM is changed from solid to liquid after absorbing the heat from batteries (electric vehicles). Due to the high thermal capacity of PCM, the PCM will remain in solid-liquid mixture state, and the temperature of the PCM around the batteries will remain constant. On the other hand, the heat stored in the PCM will be transferred to the ambient. Thus, the PCM should be chosen based on the condition that its functional temperature is higher than the surrounding one, and the functional temperature could not be higher than the working temperature of the batteries.

Sabbah et al. [16] compared the passive cooling method by using PCM with the active cooling one by forced air in a compact Li-ion battery pack. In the passive cooling, a micro-composite graphite-PCM matrix was used to surround the cells of the battery. In the active cooling, the air was blown through the gaps between the cells. When the ambient temperature was 45 ℃ and the current of battery was 3 A, both the active cooling and passive cooling could keep the battery under the limiting temperature 55 ℃. However, when the current of the battery was increased to 10 A, the active cooling could not keep the battery below 55 ℃. Contrarily, the passive cooling method was able to keep the battery below 55 ℃, as shown in Fig. 2.2. Furthermore, by using the passive cooling method, it was easy to get a uniform temperature distribution on the battery. Kizilel et al. [17] found that a failure of an individual cell was spread to the other cells, as the active cooling was used. However, by using the PCM, this failure of an individual cell would not trigger the other cells to fail. Contrarily, the temperature of the cells returned to a near-ambient value. Thus PCM is a good solution for battery cooling in vehicles.

The PCM is not only useful for cooling the batteries in electric vehicles, but also used in a combustion engine vehicle cooling system. For the diesel engine vehicle, the PCM is a good option to store the excessive heat load occurring sporadically, to reduce the size of radiator. Kim et al. [18] designed a radiator based on the average cooling power instead of the maximum one. When the maximum cooling power occurs, a heat accumulator containing PCM absorbs the heat which the small radiator can not dissipate. In this case, the small radiator and cooling fan led to a reduction of the air drag force as well as the compartment weight/volume. Meanwhile, the volume of the coolant could be reduced by 30 %, and the warm up time of a cold start was reduced as well.

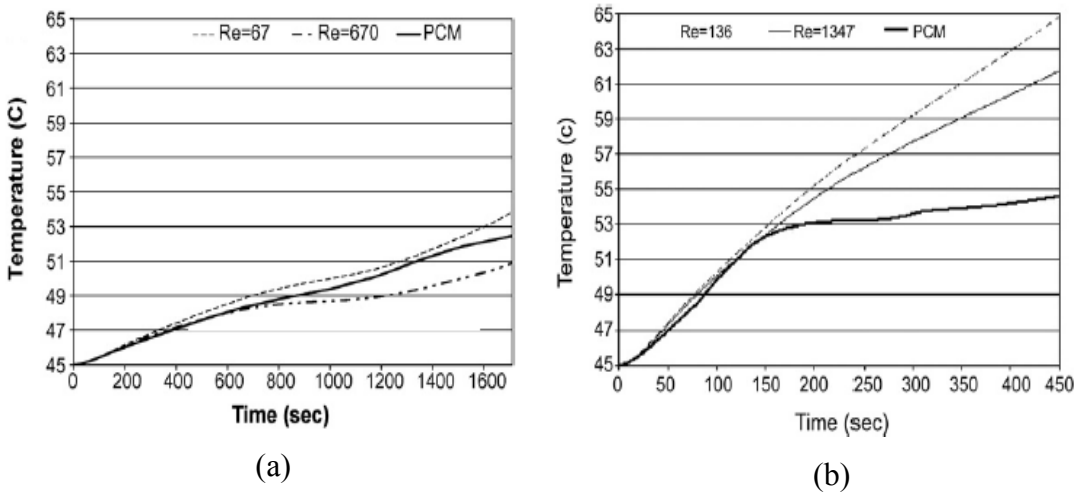

Fig. 2.2. Cooling systems based on volume averaged cell temperature at (a) 3 A; (b) 10 A. [16]

2.2.3 Rearrangement of HEXs position

In modern heavy vehicles, the amount of energy removed from the engine compartment is so large that conventional radiators and oil coolers can not handle it. Moreover, there is space limitation in the vehicle. It is extremely difficult to increase the size of the radiator to dissipate the huge heat from the engine compartment. The position of HEXs in vehicles has to be rearranged to get a chance to dissipate the huge cooling power.

Recently, the Centro Ricerche Fiat [19] tried to use some parts of the vehicle body panels as HEXs to reduce the radiator size in the light duty vehicles, as shown in Fig. 2.3. Two roll bond HEXs installed on the engine hood and below the engine could dissipate 60 % of heat from the engine in all the test conditions. On the other hand, in [20] two levels of cooling systems (high temperature system (engine radiator) and low temperature system) were introduced to a car. The intercooler and condenser were cooled by liquid instead of air. After that, the liquid was cooled by air in the low temperature system. In this case, the intercooler and condenser can be removed from the front of the vehicles to other suitable places. By introducing two levels of cooling systems, the fuel consumption in the vehicle can be reduced by 4 %.

Fig. 2.3. Different position of HEXs in a vehicle [19].

Furthermore, in [21] the thickness of the cooling package (including a radiator, a condenser, and a sub-radiator) was reduced by placing the sub-radiator on the top (instead of the front) of the condenser. Due the slim cooling package, the cooling fan power was reduced and the fuel consumption was reduced 3-5 %. Khaled et al. [22] compared the in-rank configuration of the HEXs (the HEXs are positioned differently, i.e., one is behind the other) and the in-plane configuration HEXs (the different HEXs are parallel in the flow direction). It was found that the in-plane configuration HEXs can increase the overall thermal performance by 4.4 %, and 0.9 % of the pressure losses was eliminated.

Based on the literature review, the fuel consumption could be reduced by rearranging the position of the HEXs in vehicles. The conventional radiator for heavy vehicles is always placed in the front, as shown in Fig. 2.4. If the radiator is placed at the underbody or the roof of the vehicle, it might increase the possibility to increase the radiator size for meeting the critical cooling requirement. A new configuration of the heat exchangers has to be developed to accommodate the position change. As shown in Fig. 2.4, the engine coolant flow and the air flow directions are opposite, as the radiator is placed at the roof of the driver compartment. This is a typical principle of a countercurrent flow HEX. In the vehicle industry, the engine radiator is mostly a cross flow HEX. However, a countercurrent flow HEX generally has better thermal performance than a cross flow one. Thus, placing a countercurrent flow HEX at the roof of the heavy vehicle driver compartment might be a good option for the engine radiator.

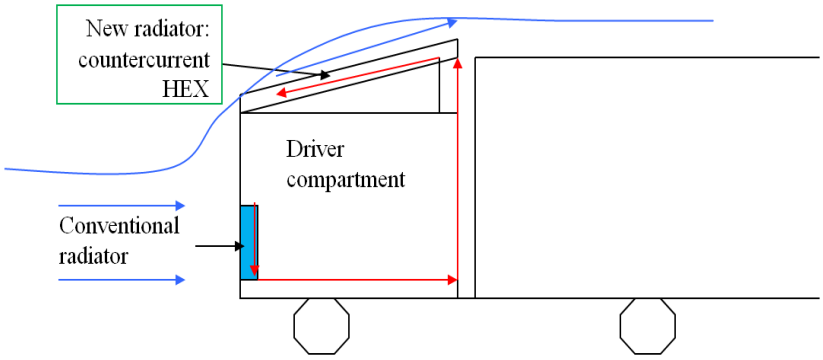

Fig. 2.4. Schematics of the positions of a radiator in trucks.

2.3 Heat exchanger/radiator

If the coolant was the blood, then the radiator would be the heart of the engine cooling system. This is to illustrate that the radiator plays a significant role in the engine cooling system. Cowell et al. [23] outlined some common constraints for the radiator design, such as compactness, low pressure drop, low weight, low cost and high volume.

2.3.1 Configurations of heat exchanger

There are two methods to increase the thermal performance of HEXs [24]. One is the passive technique, which includes special surface geometries and fluid additives. Another one is the active technique, in which the external power is required (such as

electric or acoustic fields and surface vibration). However, due to the cost, noise, safety or reliability being concerned, the active techniques are not as popular as the passive ones in the HEX commercial markets.

In the passive techniques, there are: coated surfaces, rough surfaces, extended surfaces, displaced inserts, swirl flow, coiled tubes, surface tension, additives for liquids, and additives for gas. The extended surfaces will lead to high compactness in HEXs, which is favorable for the vehicle industries.

Based on [25], the different compact surfaces (as shown in Fig. 2.5) are included in the plate-fin HEXs, as follows:

a) Rectangular fins: long uninterrupted flow passages are characterized.

b) Pin fins: the high heat transfer coefficient is achieved by maintaining thin boundary layers on the pin fins.

c) Wavy fins: due to the shape of the fins, the flow direction would be changed and the boundary-layer would be separated, which causes high thermal performance.

d) Strip fins (or offset fins): the short sections of fins are aligned entirely with the flow direction. Due to the short flow-length fins, the boundary layer never becomes thick. Thus there is a high heat transfer coefficient.

e) Perforated fins: the cut holes in perforated fins interrupt the boundary layer. Thus, the thermal performance is high with the perforated fins.

f) Louvered fins: fins are cut and bent out into the flow stream at frequent intervals, to break the boundary layers and achieve high thermal performance.

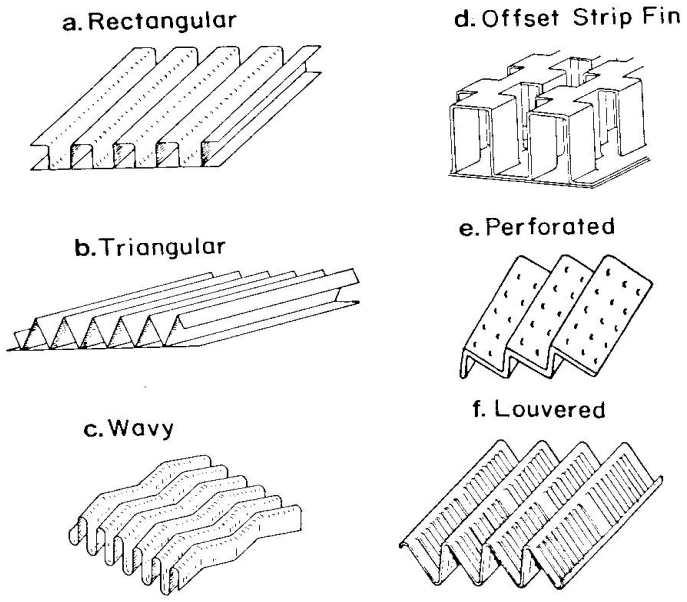

Fig. 2.5. Different configuration of fins in the plate-fin HEXs [24].

Because of the low thermal performance on the air side of the radiator, extended surface fins are placed on the air side to compensate for the low heat transfer coefficient. Nowadays, the louvered fins are favorable for the air side of a radiator. This kind of fin enormously increase the heat transfer coefficient and keep a low pressure drop on the air side, especially at high Reynolds number of the air. Oliet et al. [26] used numerical methods to carry out parametric studies for automotive radiators. The influence of some geometrical parameters (fin spacing, louver angle and so on) and the importance of coolant flow lay-out on the radiator global performance were investigated. The results showed that the air inlet temperature did not affect the overall heat transfer coefficient. Furthermore, Carluccio et al. [27] carried out a numerical study with a thermo-fluid-dynamic analysis for an air-oil compact cross flow HEX, which was used in ground vehicles. For the oil side, the geometry of the offset fins did not cause a high level of turbulence, but increased the surface area. On the air side, the wavy fins could enhance the heat transfer coefficient twice, compared to straight triangular fins.

2.3.2 New materials for heat exchangers

Another efficient method to increase the thermal performance of HEXs is the utilization of microcellular foam materials, such as metal or graphite foams. The heat transfer is enhanced by the huge fluid-solid contact surface area and the fluid mixing. Aluminum or copper heat exchangers became common in vehicles, because of their high thermal conductivity. However, the porous medium, e.g., graphite foam developed by Oak Ridge National Laboratory (ORNL) [28], has extremely high thermal conductivity. Inside the graphite foam, there are many spherical pores with small dimensions. These pores are three-dimensionally interconnected, as shown in Fig. 2.6.

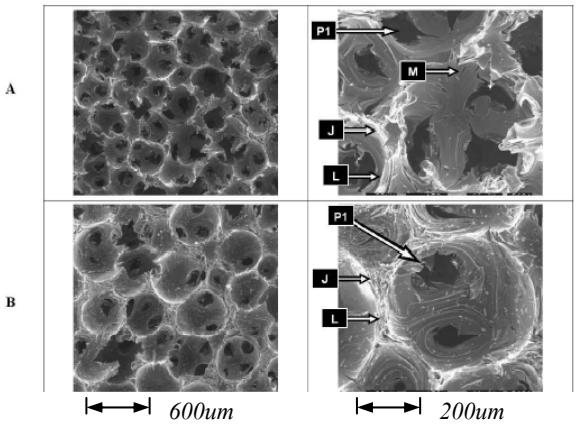

Fig. 2.6. Photomicrographs of the foams produced from Mitsubishi ARA 24 pitch at different densities, A < B (P1: opening pore; M: microcrack; J: junction; L: ligament) [29].

Because of the special structures, there are several prominent thermal properties in the graphite foam. The graphite foam made by the ORNL process exhibits high effective thermal conductivity (up to 182 W/(m·K)) and low density (0.2 - 0.6 g/cm^3). On the other hand, the data in Table 2.1 shows that the thermal conductivity in the z – plane is much larger than the one in the x – y plane. It implies that the high thermal conductivity of the graphite foam only exists in a certain direction. This is a

Table 2.1. Properties of various graphite foams made by the ORNL method compared to POCOFoam (another producer of graphite foam) [30].

	Graphitization rate (℃/min)	Average bulk density (g/cm^3)	z -Plane thermal conductivity λ_z (W/(m·K))	x-y Plane thermal conductivity λ_{xy} (W/(m·K))
ORNL graphite foam (1)	10	0.45	125	41
ORNL graphite foam (2)	1	0.59	181	60
POCOFoam™	-	0.61	182	65

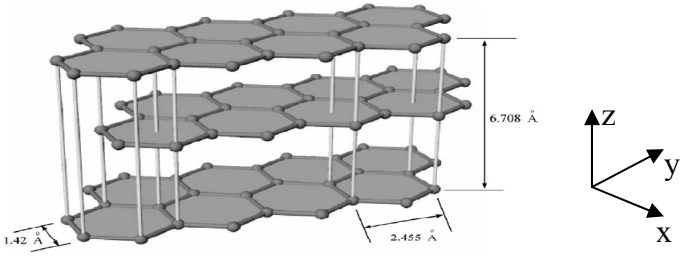

Fig. 2.7. Planar structure of hexagonal graphite [30].

disadvantage of the graphite foam. Klett et al. [30] found out that the heat inside the graphite lattice was transferred down the graphite lattice fast, because of the very stiff nature of the covalent bonds (as shown in Fig. 2.7). Moreover, the position and vibration of atoms in the neighboring planes may impede the vibration of atoms in the plane of interest. The crystal perfection controls the thermal performance. In order to achieve high thermal conductivity in the graphite crystal, the structure must be composed of aligned, straight graphene planes, and so on.

Several research works about the characteristics of graphite foams have been carried out [29, 31-32]. In summary, the characteristics of graphite foams are as follows:

1) Advantages:
    a) High thermal conductivity: The effective thermal conductivity of graphite foam is between 40 and 150 W/(m·K) [29], which is much higher than the one of an aluminum foam (between 2 and 26 W/(m·K) [33]).
    b) Low density: The density of graphite foam is from 0.2 to 0.6 g/cm^3, which is about 20 % of aluminum.
    c) Large specific surface area: Because of the open cells and inter-connected void structure, the specific surface area of graphite foam is between 5000 and 50000 m^2/m^3.
2) Disadvantages:
    a) Weak mechanical properties: The tensile strength of graphite foam is much lower than that of the metal foam.
    b) High thermal conductivity only exists in a certain direction.

Based on these characteristics, the graphite foam is a potential material for heat exchangers. Klett et al. [34] designed a radiator with carbon foam. The cross section of the automotive radiator was reduced from 48 cm x 69 cm to 20 cm x 20 cm. The reduced size could decrease the overall weight, cost and volume of the system. Yu et al. [35] proved that the thermal performance of a carbon foam finned tube radiator could be improved by 15 %, compared to a conventional aluminum finned tube radiator, without changing the frontal area, or the air flow rate and pressure drop. Furthermore, Garrity et al. [36] carried out an experimental comparison between the carbon foam heat exchanger and the multilouvered fin heat exchanger. When the volume of the heat exchangers was the same, the carbon foam samples brought away more heat than the multilouvered fin.

Even though there is a huge heat transfer enhancement in the graphite foam, the high pressure drop is the major issue facing to the graphite foam, due to the large hydrodynamic loss associated with the cell windows connecting the pores [37]. In order to reduce the pressure drop, six different configurations of graphite foam heat exchangers were presented in [38]. The solid foam had the highest pressure drop, and the finned configuration had the lowest value. On the other hand, Leong et al. [39] found that the baffle foam presented the lowest pressure drop among the four configurations of graphite foams, at the same heat transfer rate. Lin et al. [40] proved that a corrugated foam could reduce the pressure drop while maintaining a high heat transfer coefficient, compared to the solid foam. Thus, the configuration has an important effect on the pressure drop through the graphite foam.

2.3.3 Manufacturing methods of heat exchangers

For the radiator, it is very important to find a suitable manufacturing method, which can reduce the cost and improve the heat transfer performance. For instance, the brazing process is a good method for assembling a radiator in vehicles. Aluminum brazing process is to join different components by a brazing alloy (cladding) whose melting point is lower than that of the parent material (base alloy), as shown in Fig. 2.8 (a). The cladding normally is adjacent to or placed in between the components to be joined together. The brazing temperature is higher than the melting point of cladding, but lower than the melting point of parent material. In this case, the cladding material will melt and fill in the gap between different component, and form the brazed joints. There are two major kinds of brazing process. One is the flux assisted Controlled Atmosphere Brazing (CAB), another one is the vacuum brazing.

a) The flux assisted Controlled Atmosphere Brazing (CAB): The flux is to dissolve the oxide layer on the aluminum surface, in order to prevent further oxidation. Meanwhile, the flux wets the joint surface of the component, so that the filler material (cladding) could be drawn into the joints by capillary action.

b) Vacuum brazing: Due to the corrosion of flux, the vacuum brazing is introduced to eliminate the flux usage. On the other hand, in order to dissolve the oxide layer on the aluminum surface, the brazing oven has to be vacuum and strict cleaning of the aluminum surface is required before the brazing. Thus, the cost of vacuum brazing is much higher than that of CAB. However, compared to the CAB, the vacuum brazing performs a better joint between the two different components, particularly when the leakage is an important consideration.

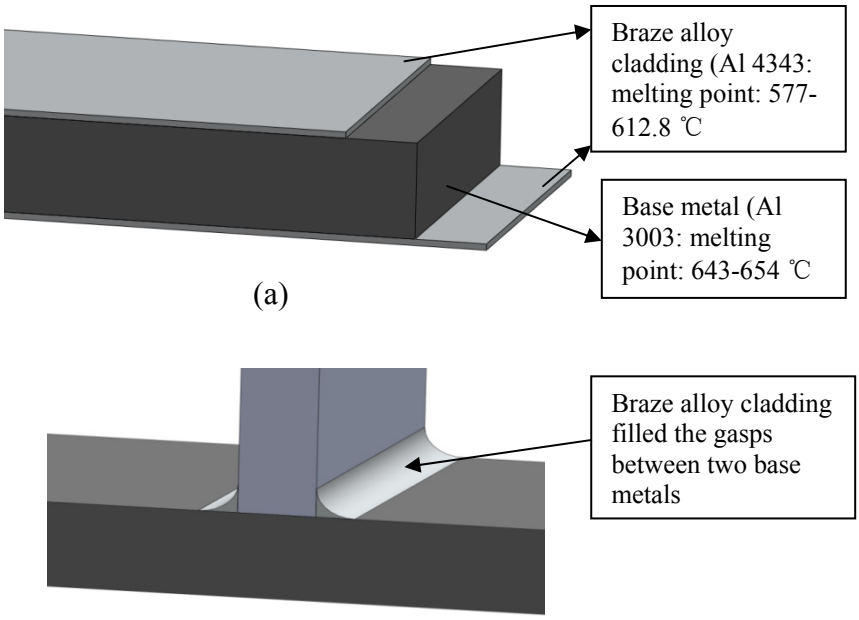

Fig. 2.8. Brazing process: (a) brazed cladding and base material; (b) product after brazing.

Witry et al. [41] introduced an aluminum roll-bonding technique for producing automotive radiators. This method was one of the cheapest ones for HEX manufacturing. In this kind of HEXs, the internal heat transfer is increased because of the repeated impingement against the dimple obstructions. The heat transfer is also increased for the external flow due to the wider and wavy nature of the surface area. As a whole, higher heat transfer levels, lower pressure drop and overall vehicle drag, smaller size radiators and cheaper manufacturing were the strengths of the roll-bonding HEX design.

2.4 Ideas of the present work

Based on the literature survey, several ideas about the engine cooling system were found to be helpful to reduce the fuel consumption in vehicles. The first one is to rearrange the position of HEXs in vehicles. In the present work, the radiator of a heavy vehicle is moved to the roof of the driver compartment. Due to the flow direction framework, a countercurrent flow HEX is developed to accommodate the new position (at the roof of driver compartment). In order to verify the performance of the countercurrent flow HEX at the roof of the truck driver compartment, an appropriate configuration of fins in HEX has to be chosen. The louver fin, wavy fin and pin fin are adopted and analyzed for the air side of a countercurrent flow HEX. Furthermore, flat tubes are used on the engine coolant side.

Meanwhile, due to the excellent thermal characteristics of graphite foam, the graphite foam HEXs could be developed to the vehicle cooling system in the present work. Because of the high flow resistance in the graphite foam, four different configurations (corrugated, wavy corrugated, pin-finned, and baffle) of the graphite foam HEXs are

analyzed, to find out which configuration of graphite foam will achieve low pressure loss and high thermal performance.

Finally the countercurrent flow HEX (made in graphite foam or aluminum) and the cross flow aluminum HEX are compared in terms of coefficient of performance (COP), power density (PD), and compactness factor (CF). A specific case study is carried out to evaluate the advantages and disadvantages of the countercurrent flow HEXs, and the impact for vehicles.

3 Modeling and numerical simulation method

Experimental or numerical methods have been employed to investigate which design of a radiator or HEX is economic and efficient. However, because of the high cost and the complexity of experiments, a numerical method is adopted in the present work to analyze the performance of HEXs. The physical model of the HEX has to be simplified and certain assumptions have to be set up. Meanwhile the governing equations and corresponding boundary conditions are introduced for the simulation model. On the other hand, the grid independence is carried out to ensure the accuracy and validity of the numerical models. At the end, several important parameters are defined for the analysis of thermal performance and pressure loss in HEXs.

3.1 Physical models and assumption

Simplified configurations of some plate-fin HEXs are shown in Figs. 3.1(a) and (b) (The schematics of a cross flow HEX are shown in Fig. 3.1 (a), and a countercurrent flow HEX is shown in Fig. 3.1 (b)). The engine coolant flows inside the flat tubes, and the air flows through fins. The heat is transmitted through the tube wall and the fins and finally dissipated to the ambient air.

Based on the literature survey, the corrugated, wavy corrugated, pin-finned, and baffle configurations are chosen for the graphite foam fins. Meanwhile, the wavy-, pin- and louver fin are adopted in the aluminum HEX. The configurations of different fins are shown in Figs. 3.1 (c) and (d).

The fluid through the HEX is assumed to be incompressible with constant properties in a steady-state. The engine coolant is assumed to be water. The thermal resistance between the water tubes and fins is neglected. The thermal conductivity of the graphite foam is assumed to be isotropic. In order to simplify the simulation model and save computational time, only a core of the HEX is adopted, as shown in Fig. 3.1 (c-d). Based on the literature survey, the overall size of the core of the graphite foam fin is: 45 mm x 12 mm x 50 mm (width (W) x height (H) x length (L)); the one of the core of aluminum fin is: 2.31 mm x 6.85 mm x 70 mm (W x H x L) [25]. The parameters of the graphite foam fins and aluminum fins are shown in Table 3.1 and Fig. 3.2, respectively. Furthermore, the parameters of the graphite foam characteristics are also shown in Table 3.2.

Table 3.1. Parameters of aluminum fins (mm).

Louver fin [25]	Fin pitch	Fin thickness	Louver spacing	Louver angle (degree)
	2.31	0.152	4.76	17.06
Wavy fin	Fin pitch	Fin thickness	Wave length	Wave amplitude
	2.23	0.152	8.9	1
Pin fin	Pin pattern	Pin diameter	Transverse spacing	Longitudinal spacing
	In-line	0.79	2.3	3.18

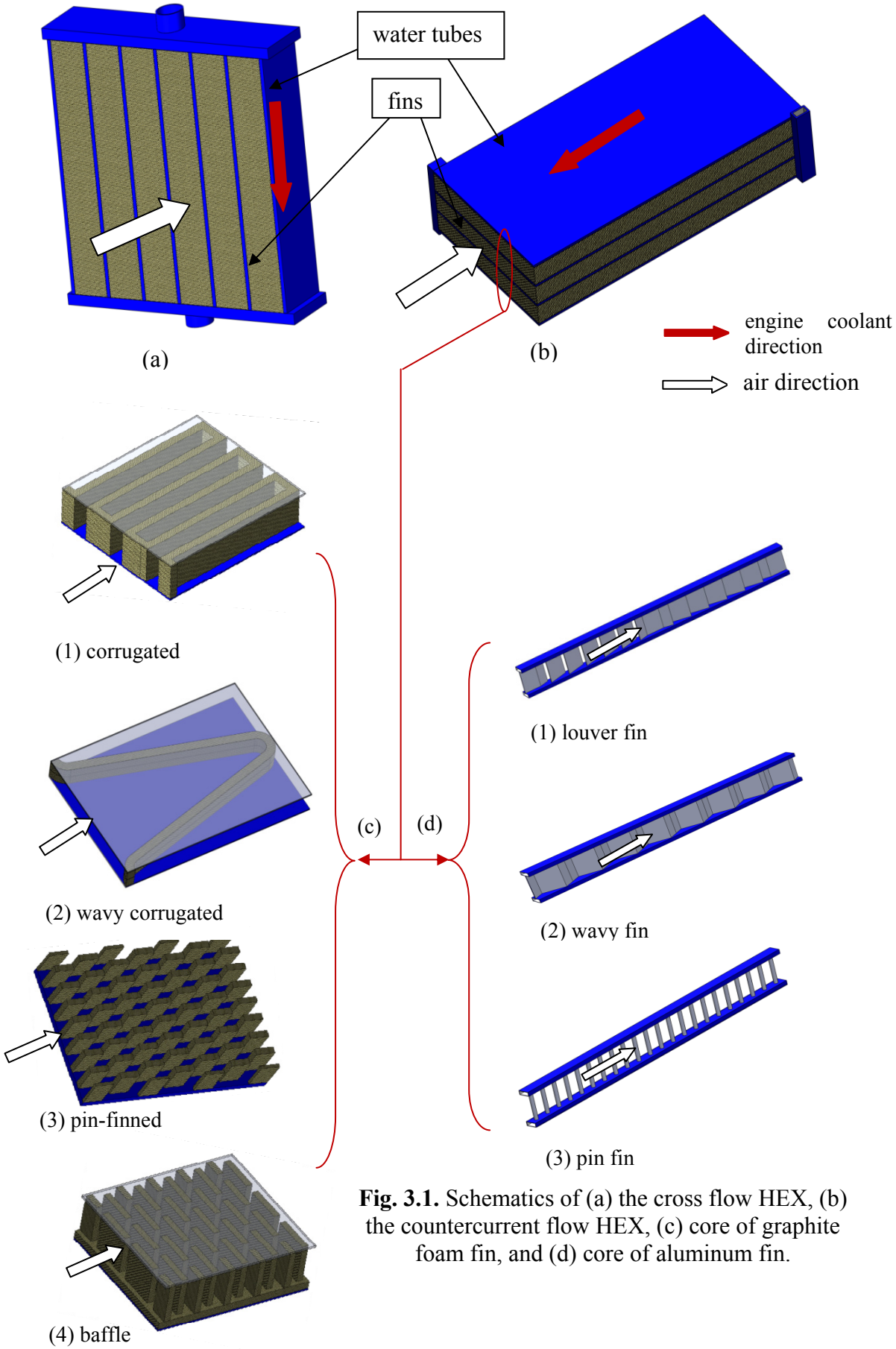

Fig. 3.1. Schematics of (a) the cross flow HEX, (b) the countercurrent flow HEX, (c) core of graphite foam fin, and (d) core of aluminum fin.

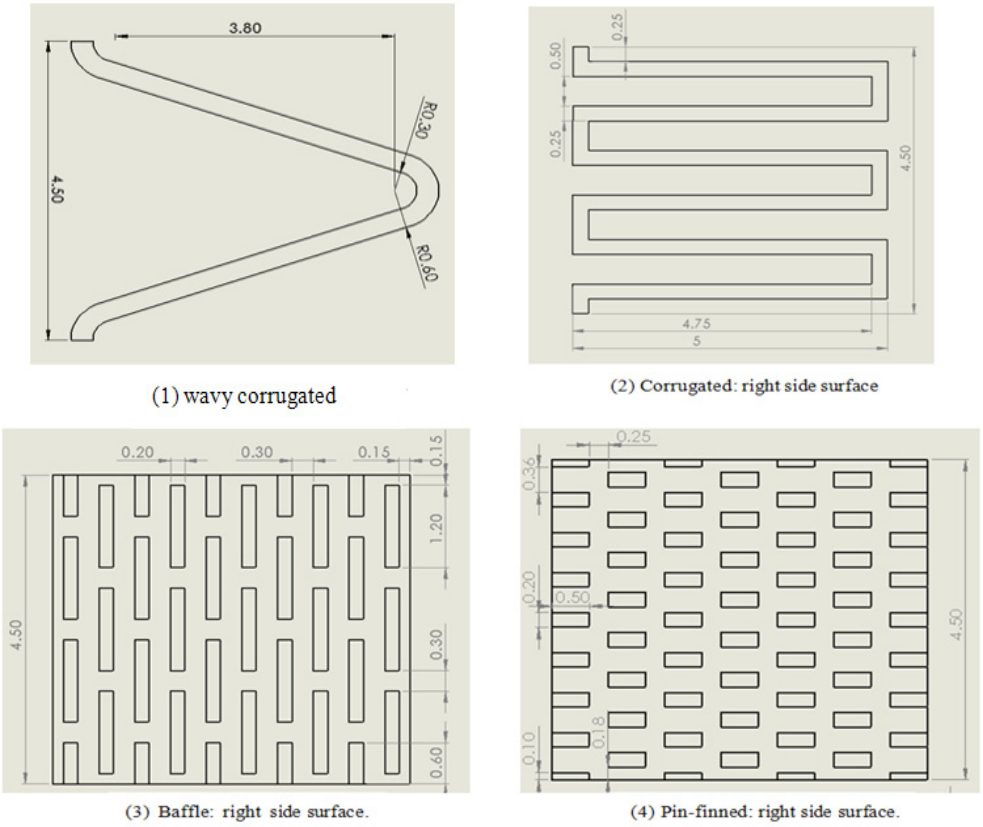

Fig. 3.2. Geometries of various graphite foams (cm).

Table 3.2. Parameters of graphite foam characteristics [37].

Graphite foam	Porosity (φ)	Density (ρ) (kg/m^3)	Area to volume ratio (γ)(m^2/m^3)	Effective thermal conductivity (λ_{eff})(W/m·K)	Permeability (α) (m^2)	Forchheimer coefficient (C_F)
POCO	0.82	500	5240	120	6.13×10^{-10}	0.4457

3.2 Adoption of flow model

In this part, a computation model (laminar or turbulent) for the flow is presented. Based on the velocity of heavy vehicles, the air inlet velocity of the countercurrent flow HEX in the study is about 50 to 70 km/h. In this case, the Reynolds number on the air side is ranging from 2300 to 13152. Thus, low Reynolds number turbulent flow prevails on the air side. In order to capture the low Reynolds characteristics in the turbulent flow, the "renormalization group" (RNG) k- ε turbulence model is adopted [42-43] on the air side. However, laminar flow prevails inside the graphite foam. This is so because it is difficult to generate turbulent eddies in the small open cells of the graphite foam. Furthermore, laminar flow is considered on the water side as well, to simplify the simulation model (the inlet velocity of water is assumed to be less than 1 m/s).

3.3 Governing equations

Based on the above mentioned assumptions, the governing equations for continuity, momentum and energy can be expressed as follows [44-46]:

3.3.1 Air zone governing equations (turbulent flow)

Continuity equation:

$$\frac{\partial(\rho_{air}u_i)}{\partial x_i} = 0 \tag{1}$$

Momentum equation:

$$\frac{\partial(\rho_{air}u_i u_j)}{\partial x_j} = -\frac{\partial p}{\partial x_i} + \frac{\partial}{\partial x_j}\left((\mu_{air} + \mu_t)\left(\frac{\partial u_i}{\partial x_j} + \frac{\partial u_j}{\partial x_i}\right)\right) \tag{2}$$

Energy equation:

$$\frac{\partial(\rho_{air}u_j T)}{\partial x_j} = \frac{\partial}{\partial x_j}\left(\left(\frac{\mu_{air}}{Pr_{air}} + \frac{\mu_t}{Pr_t}\right)\frac{\partial T}{\partial x_j}\right) \tag{3}$$

The equations for the turbulent kinetic energy k and the rate of energy dissipation ε corresponding to the RNG k- ε turbulence model are:

Turbulent kinetic energy k equation:

$$u_j\frac{\partial k}{\partial x_j} = -\overline{u_i' u_j'}\frac{\partial u_i}{\partial x_j} + \frac{\partial}{\partial x_j}\left(\frac{K_m}{\sigma_k}\frac{\partial k}{\partial x_j}\right) - \varepsilon \tag{4}$$

Rate of energy dissipation ε equation:

$$u_j\frac{\partial \varepsilon}{\partial x_j} = -C_{\varepsilon 1}\frac{\varepsilon}{k}\overline{u_i' u_j'}\frac{\partial u_i}{\partial x_j} + \frac{\partial}{\partial x_j}\left(\frac{K_m}{\sigma_\varepsilon}\frac{\partial \varepsilon}{\partial x_j}\right) - C_{\varepsilon 2}\frac{\varepsilon^2}{k} - R \tag{5}$$

where, $R = \frac{C_\mu \eta^3(1-\eta\eta_0)\varepsilon^2}{(1+\beta_0\eta^3)k}$, $\mu_t = \rho C_\mu \frac{k^2}{\varepsilon}$,

$$\eta = \frac{k}{\varepsilon}\left[\left(\frac{\partial u_i}{\partial x_j} + \frac{\partial u_j}{\partial x_i}\right)\frac{\partial u_i}{\partial x_j}\right]^{0.5},$$

$$K_m = \nu\left[1 + \left(\frac{C_\mu}{\nu}\right)^{0.5}\frac{k}{\varepsilon^{0.5}}\right]^2,$$

and the ν is the kinematic viscosity of air; u_i' are the fluctuations of the means velocity u_i.

The values of the constants are as follows:

$C_\mu = 0.0845$; $\sigma_k = 0.7179$; $\sigma_\varepsilon = 0.7179$;

$C_{\varepsilon 1} = 1.42$; $C_{\varepsilon 2} = 1.68$; $\beta_0 = 0.012$; $\eta_0 = 4.377$.

3.3.2 Water zone governing equations (laminar flow)

Continuity equation:

$$\frac{\partial(\rho_{water} u_i)}{\partial x_i} = 0 \tag{6}$$

Momentum equations:

$$\frac{\partial(\rho_{water} u_i u_j)}{\partial x_j} = -\frac{\partial p}{\partial x_i} + \frac{\partial}{\partial x_j}\left(\mu_{water}\left(\frac{\partial u_i}{\partial x_j} + \frac{\partial u_j}{\partial x_i}\right)\right) \tag{7}$$

Energy equation:

$$\frac{\partial(\rho_{water} u_j T)}{\partial x_j} = \frac{\partial}{\partial x_j}\left(\left(\frac{\mu_{water}}{Pr_{water}}\right)\frac{\partial T}{\partial x_j}\right) \tag{8}$$

3.3.3 Graphite foam zone governing equations (laminar flow)

The graphite foam is a porous media. The Forchheimer extended Darcy's law has been applied for the air pressure drop through porous media. Thus,

$$-\Delta p = \frac{\mu_{air} U}{\alpha} + \frac{\rho_{air} C_F |U| U}{\sqrt{\alpha}} \tag{9}$$

where, p is the pore pressure, μ_{air} the air viscosity, α the permeability, calculated as $\alpha = \frac{\varphi^3 d_p^2}{a(1-\varphi)^2}$, where, a is a constant to parameterize the microscopic geometry of the porous materials; φ the porosity of porous media; d_p the diameter of porous foam. ρ_{air} stands for the air density, C_F the Forchheimer coefficient, calculated as $C_F = \frac{b}{\sqrt{a\varphi^3}}$, where, b is a constant to parameterize the microscopic geometry of the porous materials. U is the air velocity inside the graphite foam pores.

There are two major models for the heat transfer of the graphite foam (porous medium) [47]. One is the thermal equilibrium model. Another one is the non-thermal equilibrium model (two-equation model). Their characteristics are as follows:

1) The thermal equilibrium model is assumed a local thermal equilibrium between fluid and solid phases. The effective thermal conductivity (λ_{eff}) has

to be chosen or calculated correctly, to ensure the accuracy of the simulation model. There are two limiting values for λ_{eff}:

$$\lambda_{eff} = \varphi\lambda_f + (1-\varphi)\lambda_s \quad \text{and} \quad \lambda_{eff} = \frac{1}{\frac{\varphi}{\lambda_f}+\frac{1-\varphi}{\lambda_s}} \tag{10}$$

The first one presents the higher limiting value of the effective thermal conductivity for the solid and fluid phases in parallel to the direction of the heat flow path. The second one is the lower limiting value for the two phases in series. For a random porous medium, the effective thermal conductivity might be a combination of these two limiting values:

$$\lambda_{eff} = c\left(\varphi\lambda_f + (1-\varphi)\lambda_s\right) + \frac{1-c}{\frac{\varphi}{\lambda_f}+\frac{1-\varphi}{\lambda_s}} \tag{11}$$

This equation could reach both limits: (1) φ=0, solid; (2) φ=1, fluid. The value c is constant to parameterize the microscopic geometry of the porous materials.

2) The two-equation model is considered when the solid and fluid are in a thermally nonequilibrium state. The heat conduction in the fluid and solid phases has to be considered separately. The interfacial heat transfer (calculated as: $q_{fs} = h_{fs}A_{sf}(\overline{T_s} - \overline{T_f})$) connects the heat transfer between the fluid and solid phases. Here, the estimation of λ_{eff} is eliminated. However, another important issue is to get a reasonable value for the interfacial heat transfer coefficient h_{fs}. If the value of h_{fs} can not be chosen or calculated correctly, then the two-equation model loses its accuracy.

In the present study, the effective thermal conductivity of the graphite foam (λ_{eff}) is based on experimental results in the literature [37] (Straatman, 2007). However, there is only little data available about the interfacial heat transfer coefficient h_{fs} for graphite foams in the literature. In order to keep the accuracy of the simulation, the thermal equilibrium model is used in this study.

Continuity equation:

$$\frac{\partial(\rho_{air}u_i)}{\partial x_i} = 0 \tag{12}$$

Momentum equations:

$$\frac{\partial\left(\rho_{air}u_iu_j\right)}{\partial x_j} = -\varphi\frac{\partial p}{\partial x_i} + \frac{\partial}{\partial x_j}\left(\mu_{air}\left(\frac{\partial u_i}{\partial x_j}+\frac{\partial u_j}{\partial x_i}\right)\right) - \varphi\left(\frac{\mu_{air}}{\alpha}u_i + \frac{\rho_{air}C_F}{\sqrt{\alpha}}|u|u_i\right) \tag{13}$$

Energy equation:

$$\varphi \frac{\partial\left(\rho_{air} c_{p.air} u_j T\right)}{\partial x_j} = \lambda_{eff} \frac{\partial}{\partial x_j}\left(\frac{\partial T}{\partial x_j}\right) \tag{14}$$

3.3.4 Aluminum fin zone (solid)

There is only energy equation in the aluminum fin zone, because it is a solid.

The energy equation reduces to:

$$0 = \lambda_{aluminum} \frac{\partial}{\partial x_j}\left(\frac{\partial T}{\partial x_j}\right) \tag{15}$$

3.4 Boundary conditions and computational domain

Only one half of the fin height is simulated, due to the symmetry in the fin height direction. Similarly, only half of the water tube is simulated in the height direction. Moreover, in order to eliminate the effect of the entrance, the computational domain is extended in the direction upstream twice the length of the HEX. Similarly, the downstream region of the HEX is extended twice the heat exchanger length, to eliminate the effect of the outlet on the flow inside the HEX. Thus, the total length of the computational domain is five times the length of the HEX, as shown in Fig. 3.3.

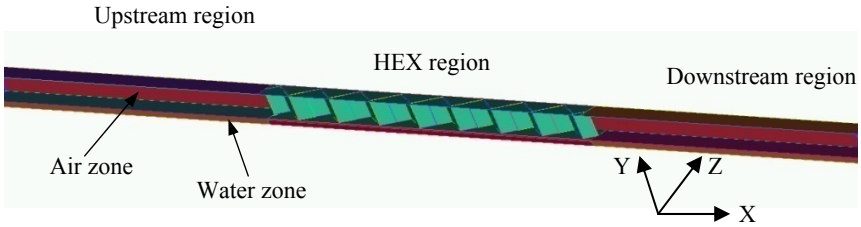

Fig. 3.3. Computational domain.

Because there are air and water zones in the simulation, the boundary conditions should be specified in the different zones separately.

1) Air zone ($H_{water} \leq Y < H$)
   a) Upstream region ($0 \leq X < 2L$):
      - Z = 0 and Z = W: $\frac{\partial u}{\partial y} = \frac{\partial v}{\partial y} = 0, w = 0, \frac{\partial T}{\partial y} = 0.$
      - Y = H: $\frac{\partial u}{\partial z} = \frac{\partial w}{\partial z} = 0, \ v = 0, \frac{\partial T}{\partial z} = 0$
      - Y = H_{water}: $u = v = w = 0, T_w = const$
      - X = 0: $u = 13\sim19\ m.s^{-1}, T = 300K, v = w = 0$
   b) Downstream region ($3L < X \leq 5L$):

- Z = 0 and Z = W: $\frac{\partial u}{\partial y} = \frac{\partial v}{\partial y} = 0, w = 0, \frac{\partial T}{\partial y} = 0$
- Y = H: $\frac{\partial u}{\partial z} = \frac{\partial w}{\partial z} = 0, v = 0, \frac{\partial T}{\partial z} = 0$
- Y = H_{water}: $u = v = w = 0, \quad T_w = const$
- X = 5L: $\frac{\partial u}{\partial x} = \frac{\partial v}{\partial x} = \frac{\partial w}{\partial x} = \frac{\partial T}{\partial x} = 0$

c) HEX region ($2L \leq X \leq 3L$):

- Z = 0 and Z = W: (1) $u_{z=0} = u_{z=W}, v_{z=0} = v_{z=W}$, $w_{z=0} = w_{z=W}, T_{z=0} = T_{z=W}$. (The geometry of the louver fin and the wavy fin is not symmetry, and periodic condition is applied.)

  (2) $\frac{\partial u}{\partial y} = \frac{\partial v}{\partial y} = 0, w = 0, \frac{\partial T}{\partial y} = 0$ (other fins)
- Y = H: $\frac{\partial u}{\partial z} = \frac{\partial w}{\partial z} = 0, v = 0, \frac{\partial T}{\partial z} = 0$
- Y = H_{water}: $u = v = w = 0, T_w = const$
- between aluminum fins and air walls are present, while between the graphite foam fins and the air, interior surfaces appear.

2) Water zone ($0 \leq Y < H_{water}$)

d) Upstream region ($0 \leq X < 2L$):

- Z = 0 and Z = W: $\frac{\partial u}{\partial y} = \frac{\partial v}{\partial y} = 0, w = 0, \frac{\partial T}{\partial y} = 0$
- Y = 0: $\frac{\partial u}{\partial z} = \frac{\partial w}{\partial z} = 0, v = 0, \frac{\partial T}{\partial z} = 0$
- Y = H_{water}: $u = v = w = 0, \quad T_w = const.$
- X = 0: $\frac{\partial u}{\partial x} = \frac{\partial v}{\partial x} = \frac{\partial w}{\partial x} = \frac{\partial T}{\partial x} = 0$ (outlet)

e) Downstream region ($3L < X \leq 5L$):

- Z = 0 and Z = W: $\frac{\partial u}{\partial y} = \frac{\partial v}{\partial y} = 0, w = 0, \frac{\partial T}{\partial y} = 0$
- Y = 0: $\frac{\partial u}{\partial z} = \frac{\partial w}{\partial z} = 0, v = 0, \frac{\partial T}{\partial z} = 0$

  Y = H_{water}: $u = v = w = 0, \quad T_w = const$

  X = 5L: $u = 0.5\, m.s^{-1}, \quad T = 350K, \quad v = w = 0$

f) HEX region ($2L \leq X \leq 3L$):

- Z = 0 and Z = W: $\frac{\partial u}{\partial y} = \frac{\partial v}{\partial y} = 0, w = 0, \frac{\partial T}{\partial y} = 0$
- Y = 0: $\frac{\partial u}{\partial z} = \frac{\partial w}{\partial z} = 0, v = 0, \frac{\partial T}{\partial z} = 0$
- X = 0: $u = v = w = 0, T_w = const$

3.5 Numerical methods

The commercial code ANSYS FLUENT 12.0 is used for the numerical solution. The finite volume method (FVM) is adopted to convert the governing equations to algebraic equations, so that they can be solved numerically [48]. The Semi-Implicit Method for Pressure Linked Equations (SIMPLE) algorithm is used to couple pressure and velocity. A second-order upwind scheme is used for the space discretization of the momentum, energy and turbulence equations in the simulations. The convergence criterion for continuity, momentum, k and ε equations is below 10^{-3}. However, for the energy convergence needs to satisfy also the energy balance

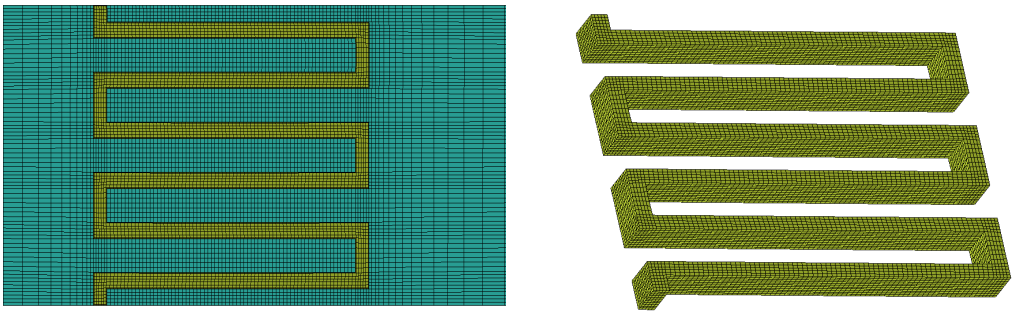

(a) (b)

Fig. 3.4. Meshing for the computations: (a) 2-D cross-sectional view; (b) 3-D on fin surfaces.

between the air zone and the water zone under the countercurrent flow condition. Thus, the convergence criterion for energy is below 10^{-8}.

The mesh generation is carried out by the preprocessor-software ICEM. There are two major techniques in the mesh generation. One is the blocking technique (mostly for Hexa Meshing, as shown in Fig. 3.4). Another one is the auto meshing technique. The HEX region occupies most of cells (60 ~ 70 % of the whole computational domain).

Table 3.3. Grid independence study based on Δp (G: graphite foam; Al: aluminum; (frontal velocity is 14 m/s).

	Case 1		Case 2		Case 3		Δp deviation (%)
	Grid (L-W-H)	Δp (Pa)	Grid (L-W-H)	Δp (Pa)	Grid (L-W-H)	Δp (Pa)	
Pin-finned (G)	*(63-79-19)*	2510	*(93-79-19)*	2610	*(113-79-19)*	2610	3.8
Corrugated (G)	*(49-81-11)*	2872	*(75-81-11)*	2930	*(75-81-19)*	2938	0.3 - 2.2
Stagger (G)	*(99-83-11)*	38932	*(99-83-17)*	38788	*(121-83-17)*	38989	0.15 - 0.5
Wavy corrugated (G)	*(139-100-15)*	2236	*(139-100-21)*	2263	*(150-100-21)*	2309	2 - 3.2
Wavy fin (Al)	*(300-21-33)*	726	*(337-21-33)*	742	*(367-25-38)*	755	1.7 - 3.8
Louver fin (Al)	(233-17-12)	438	(350-17-12)	444	(350-30-12)	448	0.9 - 2.1
Pin fin (Al)	(313-15-23)	784	(313-29-25)	798	(441-29-25)	804	0.7 - 2.5

To ensure the accuracy and validity of the numerical models, a careful check of the grid dependence of the numerical solutions has been carried out by considering three grid systems to the aluminum HEX and the graphite foam HEX. The results of the grid study for different HEXs are shown in Tables 3.3 and 3.4. It is found that the relative deviation of the pressure drops among the three sets of the grid system is less than 2.2 % in the graphite foam corrugated fin. Furthermore, the relative deviation of

the heat transfer coefficients between the three sets of grid system is less than 3 % in the graphite foam corrugated fin. Thus, in order to save computational time and keep the accuracy of the simulation, the Case 2 mesh system is chosen for the graphite foam corrugated fin. The same method was adopted to check the grid independence of other configurations of fins. At the end, the Case 2 grid system is chosen for all the fins.

Table 3.4. Grid independence study based on *h* (frontal velocity is 14 m/s).

	Case 1		Case 2		Case 3		*h* deviation (%)
	Grid	*h* (W/m^2·K)	Grid	*h* (W/m^2·K)	Grid	*h* (W/m^2·K)	
Pin-finned (G)	*(63-79-19)*	431.24	*(93-79-19)*	400.52	*(113-79-19)*	402.60	0.5 - 7.1
Corrugated (G)	*(49-81-11)*	259.26	*(75-81-11)*	263.40	*(75-81-19)*	267.04	1.4 - 3
Stagger (G)	*(99-83-11)*	450.10	*(99-83-17)*	454.46	*(121-83-17)*	461.49	1.5 - 2.5
Wavy corrugated (G)	*(139-100-15)*	1077.6	*(139-100-21)*	1088.2	*(150-100-21)*	1100	1.1 - 2
Wavy fin (Al)	*(300-21-33)*	183.44	*(337-21-33)*	188.5	*(367-25-38)*	192	1.8 - 4.4
Louver fin (Al)	(233-17-12)	220.3	(350-17-12)	225.3	(350-30-12)	228.3	1.3 - 3.5
Pin fin (Al)	(313-15-23)	225.63	(313-29-25)	236.53	(441-29-25)	241.85	2.2 - 6.7

3.6 Definition of parameters

Before analyzing and comparing the fluid flow and heat transfer characteristics for different configurations of the HEX (graphite foam HEX, aluminum HEX), several parameters have to be defined. The thermal performance can be characterized by the Nusselt number (Nu), or Stanton number (St) [49].

$$Re = \frac{\rho_f \cdot u_{max} \cdot D_h}{\mu} \tag{16}$$

$$h_f = \frac{Q}{A_0 \Delta T} \tag{17}$$

$$Nu = h_f \cdot \frac{D_h}{\lambda_f} \tag{18}$$

$$St = \frac{h_f}{\rho_f \cdot u_{max} \cdot c_p} \tag{19}$$

Q is the total amount of heat dissipated to air (W); A_0 the fin surface area (m^2), for the graphite foam $A_0 = \gamma V$ (γ is the area to volume ratio, m^2/m^3; V the volume of graphite

foam, m^3); $\triangle T$ the logarithmic mean temperature difference, LMTD (K); and D_h the hydraulic diameter (m), for the graphite foam it is the diameter of the foam (d_p). These are defined as follows:

$$Q = m \cdot c_p \cdot (T_{out} - T_{in}) \tag{20}$$

$$\Delta T = \frac{(\Delta\, T_{max} - \Delta\, T_{min})}{ln \frac{\Delta\, T_{max}}{\Delta\, T_{min}}} \tag{21}$$

$$\Delta T_{max} = max\left(T_{out}^{water} - T_{in}^{air}, T_{in}^{water} - T_{out}^{air}\right) \tag{22}$$

$$\Delta T_{min} = min\left(T_{out}^{water} - T_{in}^{air}, T_{in}^{water} - T_{out}^{air}\right) \tag{23}$$

$$D_h = \frac{4A_c}{C} \tag{24}$$

where, T_{in} and T_{out} are the bulk temperatures at the inlet and outlet section of the HEX region, respectively, (K); A_c the minimum free-flow area (m^2); C the wetted perimeter of the minimum free-flow channel, (m);

The fluid flow characteristics can be evaluated by the pressure drop ($\Delta\, p$) and friction factor (f).

$$\Delta p = p_{in} - p_{out} \tag{25}$$

$$f = \frac{A_c}{A_0} \cdot \frac{2\Delta p}{\rho_f (u_{max})^2} \tag{26}$$

where, p_{in} and p_{out} are the bulk pressure at the inlet and outlet section of the HEX region, respectively, (Pa).

4 Results and discussion

The thermal performance and the pressure loss are the two important parameters in the heat exchanger design. In order to develop a high performance countercurrent flow HEX, different configurations of fins (aluminum HEX: louver-, wavy- and pin fin; graphite foam HEX: corrugated-, wavy corrugated-, pin-finned- and baffle fin) are simulated on the air side. Flat tubes are used on the water side. The thermal performance and the pressure loss are predicted by using ANSYS FLUENT. In addition, an overall performance comparison is carried out between the countercurrent flow (made in graphite foam or aluminum) and the cross flow aluminum HEXs, in terms of coefficient of performance (COP), compactness factor (CF) and power density (PD).

4.1 Validation of models

Prior to presenting the simulation results, it is important to validate the computational models. There are two models in the present work, i.e., the graphite foam fin model and the aluminum fin model.

4.1.1 Validation of the graphite foam fin model

In order to compare the simulation results with the experimental data in [37], a block graphite foam with the size of 6 mm (width) x 50 mm (height) x 50 mm (length) is simulated. The coolant through the graphite foam block is however water instead of air (in the air zone), and a constant temperature is specified at the base of the graphite foam block. The pressure drop (Δp) and Nu number were compared with the experimental results in [37], as shown in Table 4.1. It is found that the largest deviation of the Nusselt number between the simulation (laminar flow: the frontal velocity was chosen based on the one in the experimental work [37]) and the experimental result is less than 7.1 %, and the lowest deviation is around 1.9 %. The deviation of the pressure drops between the simulation and the experimental data is less than 3 %. It should be noted that no information on experimental uncertainty of the Nu number was supplied in the experimental work [37]. Based on the maximum deviation (7.1 % in the Nusselt number, 3 % in the pressure drop), it is believed that the present model is satisfactory and applied further to estimate the graphite foam pressure drop and the thermal performance.

Table 4.1. Deviation between the simulation and the experimental data (graphite foam)

Frontal velocity (m/s)	Nu number in [37]	Nu number predicted in this study	Δp in [37] (kPa)	Δp predicted (kPa)
0.009	40	38 (5 %)	1.0	1.029 (2.9 %)
0.03	100	101.9 (1.9 %)	3.5	3.41 (2.6 %)
0.048	122	130 (6.5 %)	7.0	6.9 (1.4 %)
0.069	140	150 (7.1 %)	11.2	10.9 (2.7 %)

4.1.2 Validation of the aluminum fin model

The louver fin is adopted in the validation of the aluminum fin model. In order to compare the simulation results of the louver fin with the experimental data [25] which was obtained for cross flow conditions, the water zone in the simulation is assumed to be at a constant temperature. The comparison of $StPr^{2/3}$ and the friction factor f between the simulation and the experimental results is shown in Table 4.2. The deviation of the $StPr^{2/3}$ between the simulations by the RNG k- ε turbulence model and the experimental data is less than 5.4 %, and the deviation of the friction factor f is less than 4.1 %. In the experimental work by Kays [25], the experimental uncertainty of the $StPr^{2/3}$ value was ± 5.0 %, and the one in the friction factor f ± 5.0 %. Thus, there is a good agreement between the simulation and the experiment, in terms of thermal performance and pressure loss.

Table 4.2. Deviation between the prediction and the experimental data (aluminum louver fin).

Re	$StPr^{2/3}$ in [25]	Simulation $StPr^{2/3}$	f in [25]	Simulation f
2837	0.0092	0.0097 *(5.4 %)*	0.0435	0.044 *(1.1 %)*
3392	0.0087	0.0086 *(1.2 %)*	0.041	0.04 *(2.4 %)*
3769	0.0082	0.0081 *(1.2 %)*	0.0398	0.0382 *(4.1 %)*

4.2 Performance comparison among three configurations of aluminum fin

In the present work, a countercurrent flow HEX is proposed to accommodate with the HEX position change (the radiator would be removed to the roof of the driver compartment). Three different configurations (pin-, wavy- and louver fin) of aluminum fin are analyzed in terms of pressure loss and the thermal performance, to evaluate which configuration may achieve a good performance.

4.2.1 Pressure loss

The pressure drop through the three configurations of fins (louver-, wavy- and pin fin) varies with frontal air velocity, as shown in Fig. 4.1. As expected, the pressure drops increase with increasing air velocity. Among the three configurations of the fins, the louver fin shows the lowest pressure drop. It implies that the flow resistance in the louver fin is lower than that of the wavy and the pin fins.

Moreover, by taking account of the dimensionless parameter – friction factor (f), the friction factor is reduced with increasing Re number. The louver fin has the lowest value of the friction factor f among the three cases (as shown in Fig. 4.2), due to the low flow resistance in the louver fin.

Based on Fig. 4.3 (a), the flow through the louver fins becomes parallel to the louvers at high velocity. In this case, the louver fins behave like a flat plate, and the air flow path is smooth due to the "flat plate". Thus, the flow resistance is very low in this configuration. However, the flow has to change its direction in the wavy fin, due to the structure of the wavy fin (as shown in Fig. 4.3 (b)). This effect leads to a high

flow resistance in the wavy fins. On the other hand, Fig 4.3 (c)-(d) show that the flow has to go around the pin fins, because of the round shape of the pin fins. A high flow resistance is presented in the pin fin as well. Furthermore, it is found that the velocity is more uniform in the louver fin (Fig. 4.3 a) than the one in the wavy fin (Fig. 4.3 b) or the pin fin (Fig. 4.3 c). This means that the kinetic energy does not change significantly in the louver fin. Thus, the pressure variation is small in the louver fin configuration, compared to the wavy- and the pin fin configurations. In other words, the pressure drop through the louver fin is much lower than the one through the wavy fin and the pin fin.

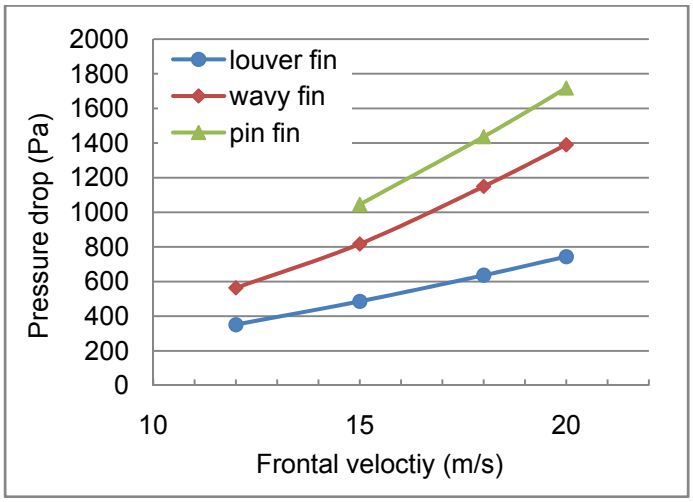

Fig. 4.1. Pressure drop vs. frontal velocity.

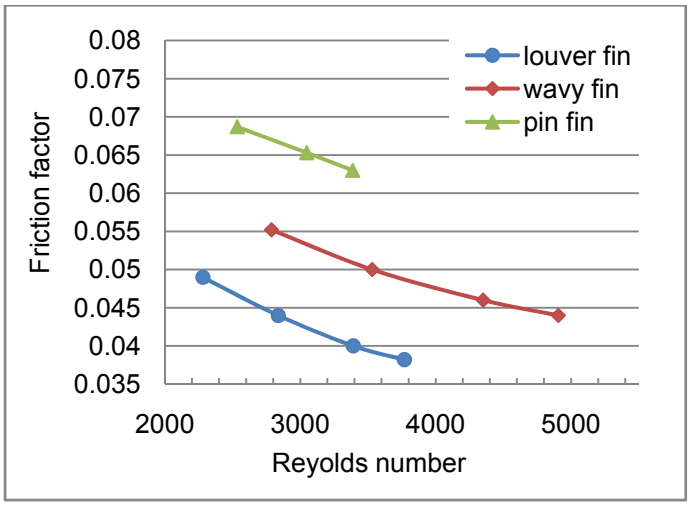

Fig. 4.2. Friction factor vs. Reynolds number.

4.2.2 Thermal performance

The heat transfer coefficients predicted for the three configurations of the fins are shown in Fig. 4.4. The heat transfer coefficient is correlated with the frontal velocity of air. Among these three configurations of the fins, the louver and pin fins present higher heat transfer coefficients than the wavy fin. The boundary layers have significant effect on the thermal performance of different configurations. As shown in

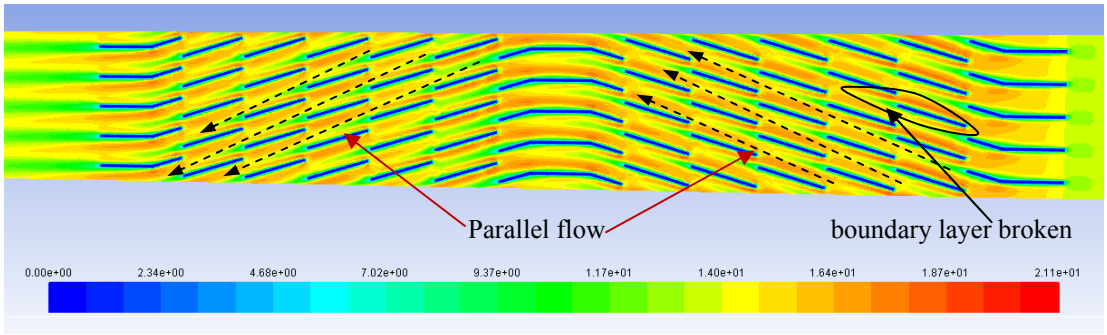

(a)

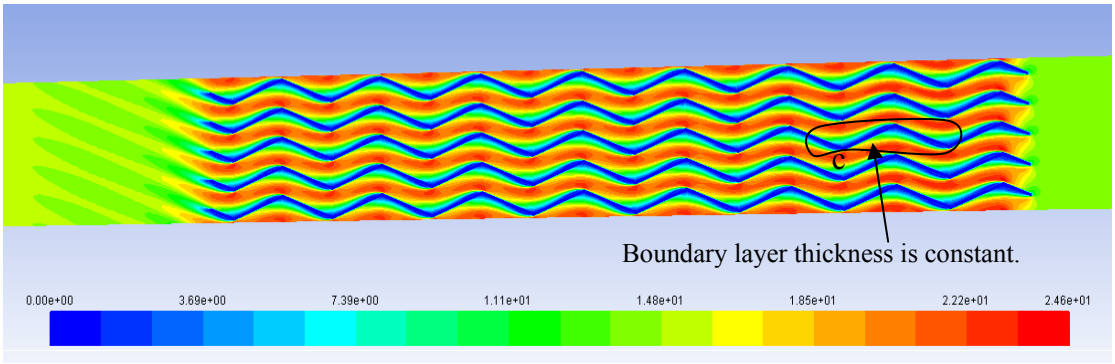

(b)

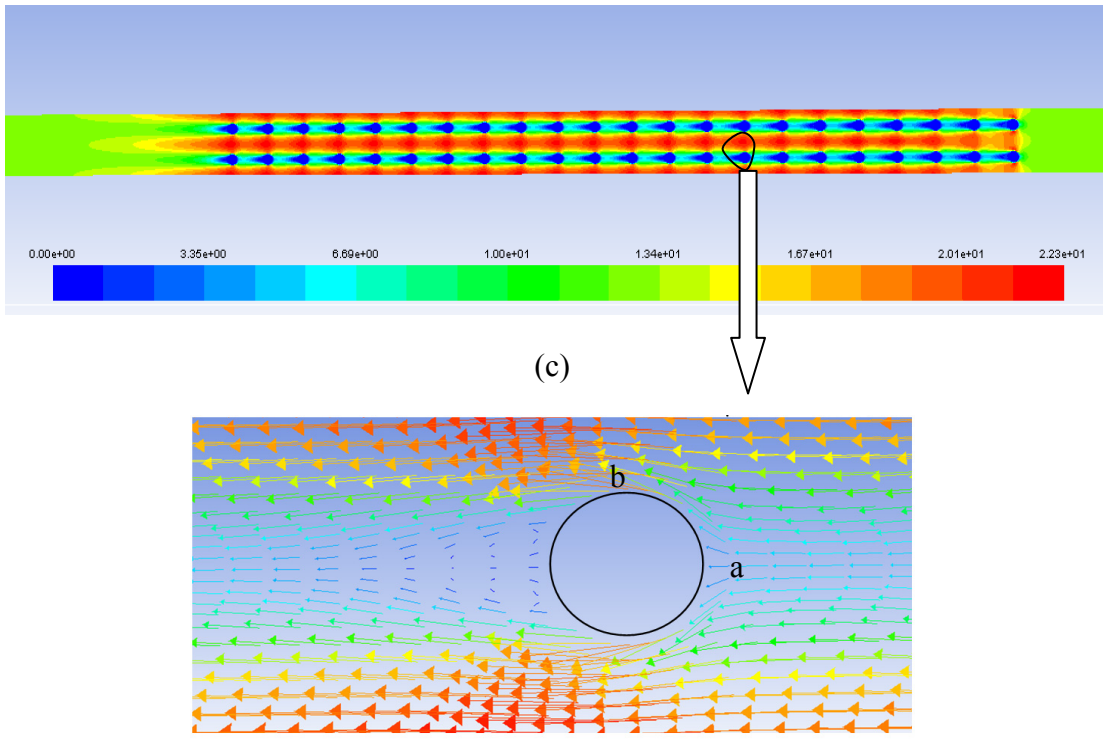

(c)

(d)

Fig. 4.3. Velocity predicted for: (a) louver fin; (b) wavy fin; (c) pin fin; and (d) around a pin fin. (at air inlet velocity of 12 m/s)

Fig. 4.3 (a), the boundary layer is developed along the louver fins. However, at the end of the fins, the developed boundary layer is broken by the vacancy of fins. Thus, the boundary layer in the louver fins never becomes thick at the high air speed. This leads to a high heat transfer coefficient around the louver fins. On the other hand, the boundary layer is developed from point *a* to *b* on the pin fin (as shown in Fig. 4.3 (d)). After the point *b*, the boundary layer separates from the pin fin. In this case, the boundary layer is thin. Thus, a high heat transfer coefficient is revealed around the pin fin as well. For the wavy fin configuration, the boundary layer is developed along the wavy fins. Due to the wavy configuration, the thickness of boundary layer on one side of the fin is reduced after point *c* (Fig. 4.3 (b)). However, the boundary layer becomes thick on the other side of the fin at the same time. Thus, the total thickness of boundary layer around the wavy fin is kept almost constant. In this case, the heat transfer coefficient is not enhanced as much as in the configurations of the louver and the pin fins (as shown in Fig. 4.4).

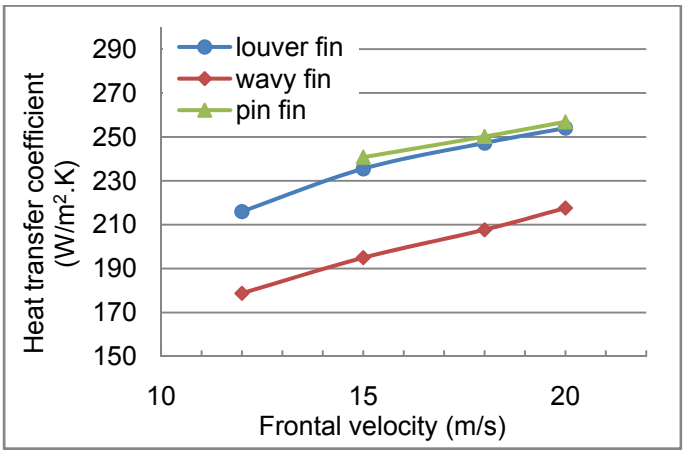

Fig. 4.4. Heat transfer coefficient vs. frontal velocity.

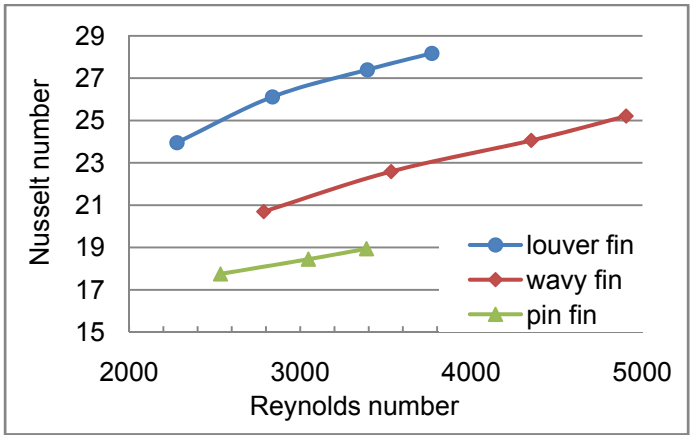

Fig. 4.5. Nusselt number vs. Reynolds number.

The dimensionless parameters (Nu number and Re number) are introduced to analyze the heat exchanger performance, in order to eliminate the effect of different sizes of the fins. Fig. 4.5 illuminates the relationship between the Nu number and the Re number among the wavy-, pin- and louver fins. The louver fin shows a higher Nu number than the wavy and the pin fins at the same Re number. Even though the heat

transfer coefficients are similar between the pin fin and the louver fin (Fig. 4.4), due to the in-line fin pattern and the small hydraulic diameter in the pin fin, the Nu number is much lower for the pin fin than for the louver fin. Based on Fig. 4.4 and Fig. 4.5, it is revealed that the louver fin provides better thermal performance than the wavy fin and the pin fin.

4.3 Performance comparison among four configurations of graphite foam

Due to the high thermal conductivity and low density, the graphite foam is a good material for HEX. However, the high pressure loss is the major issue to block the development of graphite foam HEXs. In order to find an appropriate configuration for the graphite foam fin, four different configurations (corrugated-, wavy corrugated-, pin-finned-, and baffle) of graphite foam fins are considered in the present work. To simplify the simulation in the graphite foam HEXs, only the air zone is considered. A constant temperature is set on the base of the graphite foam fin. The pressure loss and the thermal performance of different configurations of graphite foam fins are analyzed and discussed in this part.

4.3.1 Pressure loss

The pressure loss through the graphite foam is based on the Forchheimer extended Darcy's equation:

$$-\Delta p = \frac{\mu_{air} U}{\alpha} + \frac{\rho_{air} C_F |U| U}{\sqrt{\alpha}} \tag{27}$$

According to the Forchheimer extended Darcy's equation, the pressure drop through the graphite foam is increased with increasing frontal velocity, as shown in Fig. 4.6. However, the pressure drop through the baffle graphite foam increases faster than for the other cases, as the frontal air velocity is increased. Furthermore, the pressure drop through the baffle graphite foam is approximately 10 times higher than the other cases. This implies that the flow resistance in the baffle configuration is much higher than for the other cases.

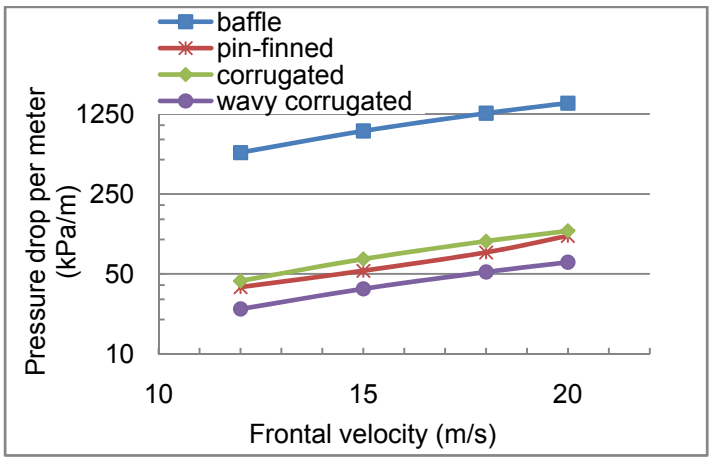

Fig. 4.6. Pressure drop through four configurations of foam fins.

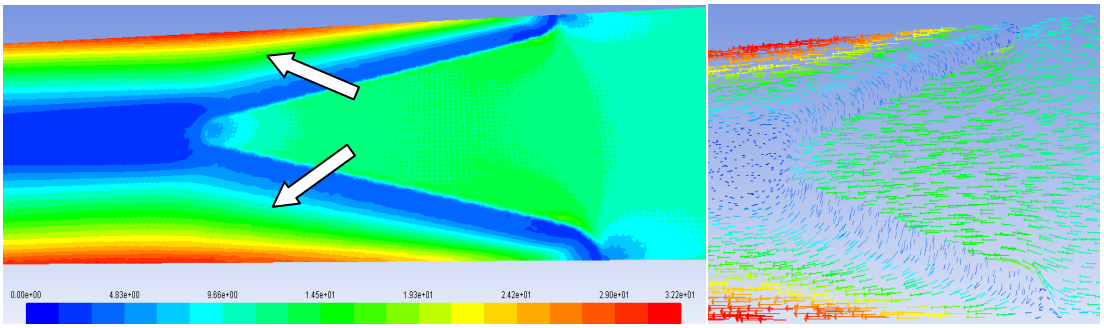

(a)

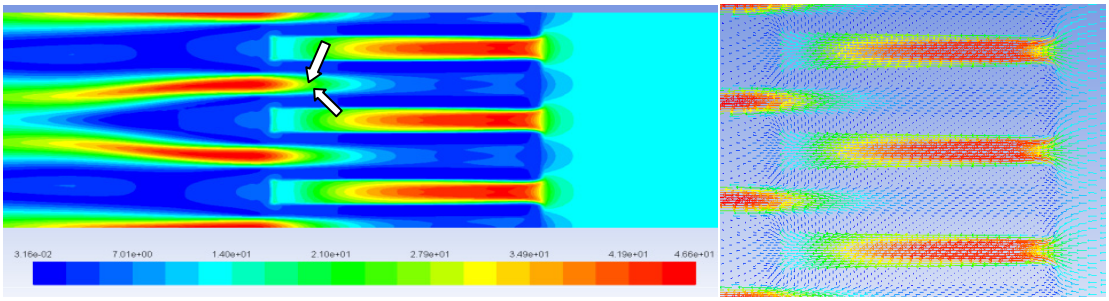

(b)

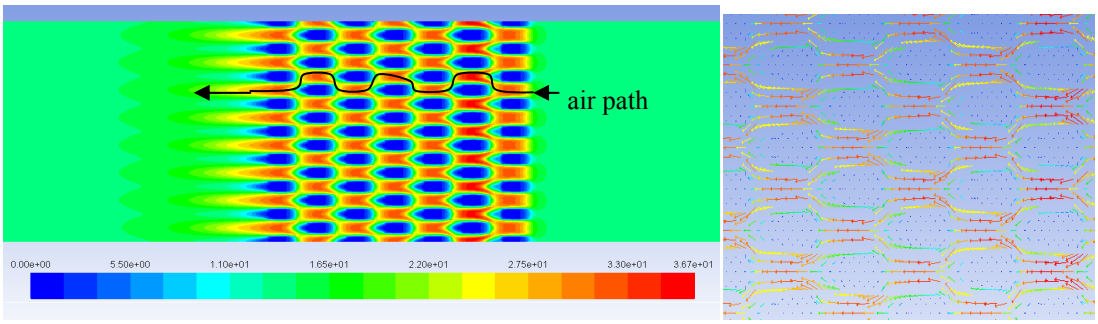

(c)

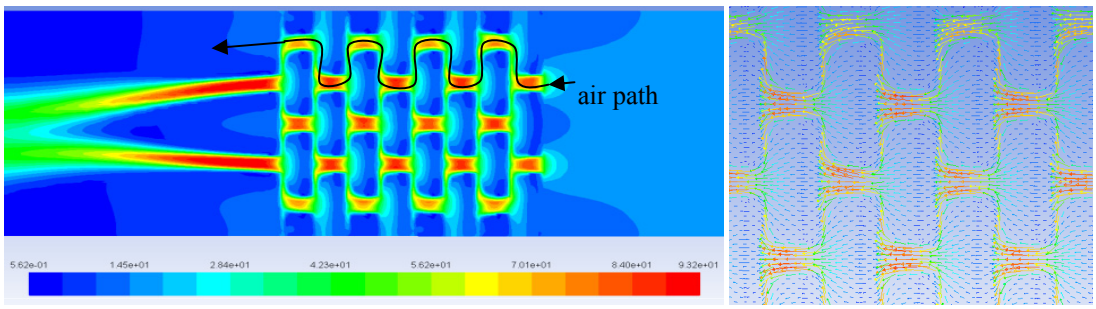

(d)

Fig. 4.7. Velocity distribution contours and vectors among different graphite foam fins at 12 m/s inlet velocity: (a) wavy corrugated fin; (b) corrugated fin; (c) pin-finned fin; (d) baffle fin. (m/s)

The major factors affecting the pressure drop through the graphite foam fins are the air length inside the foam and the air path. As shown in Fig. 4.7, all the air has to pass through the corrugated and the wavy corrugated foams (Figs. 4.7 a and b). However, due to the short flow length (the flow length inside the corrugated foam is 2.5 mm, the one of the wavy corrugated foam 3 mm), the pressure drop through the wavy corrugated foam fin or the corrugated foam fin is low. For the other cases, the major

amount of air bypasses the foam instead of passing through the baffle and the pin-finned foams, as shown in Figs. 4.7 c and d. Because the flow path around the pin-fins is much smoother than the one around the baffle fins, the pressure drop of the pin-finned foam is much lower than that for the baffle fins. Moreover, due to the air flow path of the baffle fins, a large amount of air is forced to pass through the baffle graphite foam fins. Thus, a high flow resistance is produced in the baffle fins, compared to other configurations of the graphite foam fins. In other words, the baffle fin presents the highest pressure drop among the considered four configurations.

4.3.2 Thermal performance

The heat transfer coefficients predicted for the four configurations of graphite foam fins are shown in Fig. 4.8. The heat transfer coefficient is correlated with the frontal velocity of air. Among these four configurations, the wavy corrugated fin provides much higher heat transfer coefficient than the other configurations. In addition, the heat transfer coefficient is increased much faster for the wavy corrugated fin than for the other fins, as the air frontal velocity increases.

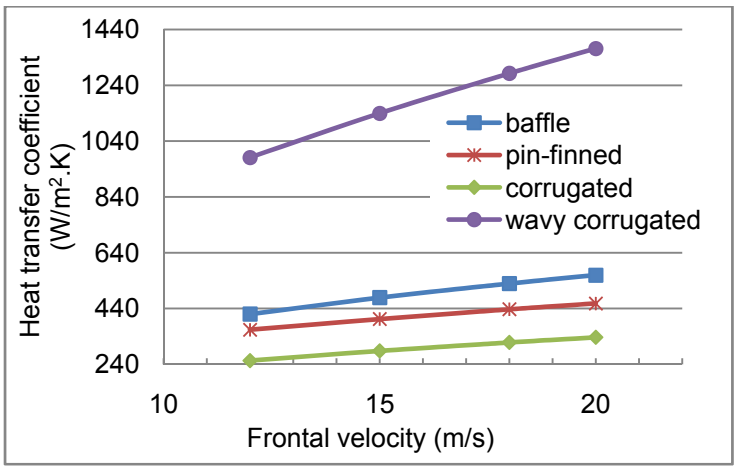

Fig. 4.8. Heat transfer coefficients of four configurations of foam.

By taking account of Fig. 4.9, an in-depth understanding of the thermal performance may be found. Figs. 4.9 (a) and (b) show that the fresh air was pre-heated before it reaches the inside of the graphite foam fin due to the heat from the nearby fins. The space between two fins is much larger for the wavy corrugated fin than for the corrugated fin. Thus, the pre-heating effect is much less in the wavy corrugated fin than in the corrugated fin. Due to the pre-heating effect, the temperature difference between the fin and the air is reduced. The reduced temperature difference decreases the thermal performance. Thus, the heat transfer coefficient inside the corrugated foam is much less than that of the wavy corrugated foam.

Based on Fig. 4.9 (c) and (d), the temperature of air increases along the length of the fins. Fig 4.9 (c) shows that the air temperature (after the pin-finned foam) is lower than that of the fin. This implies that the length of the pin-finned foam is too short to achieve the fully thermal developed regime. However, the fully thermal developed regime is attained within the length of the baffle foam, based on Fig. 4.9 (d). Thus, the

baffle foam provides a higher heat transfer coefficient than the pin-finned. Another interesting result is that the length of the baffle foam could be shorten, while that of the pin-finned should be extended, to reach the thermal fully developed regime.

As discussed above, the corrugated fin has a higher pressure drop or flow resistance than the pin fin. It is difficult for the cold air to reach the surface inside the foam and bring away the heat from the foam. Thus, the effective surface heat transfer is reduced significantly in the corrugated foam. This effect causes a lower heat transfer coefficient in the corrugated foam than in the pin-finned foam.

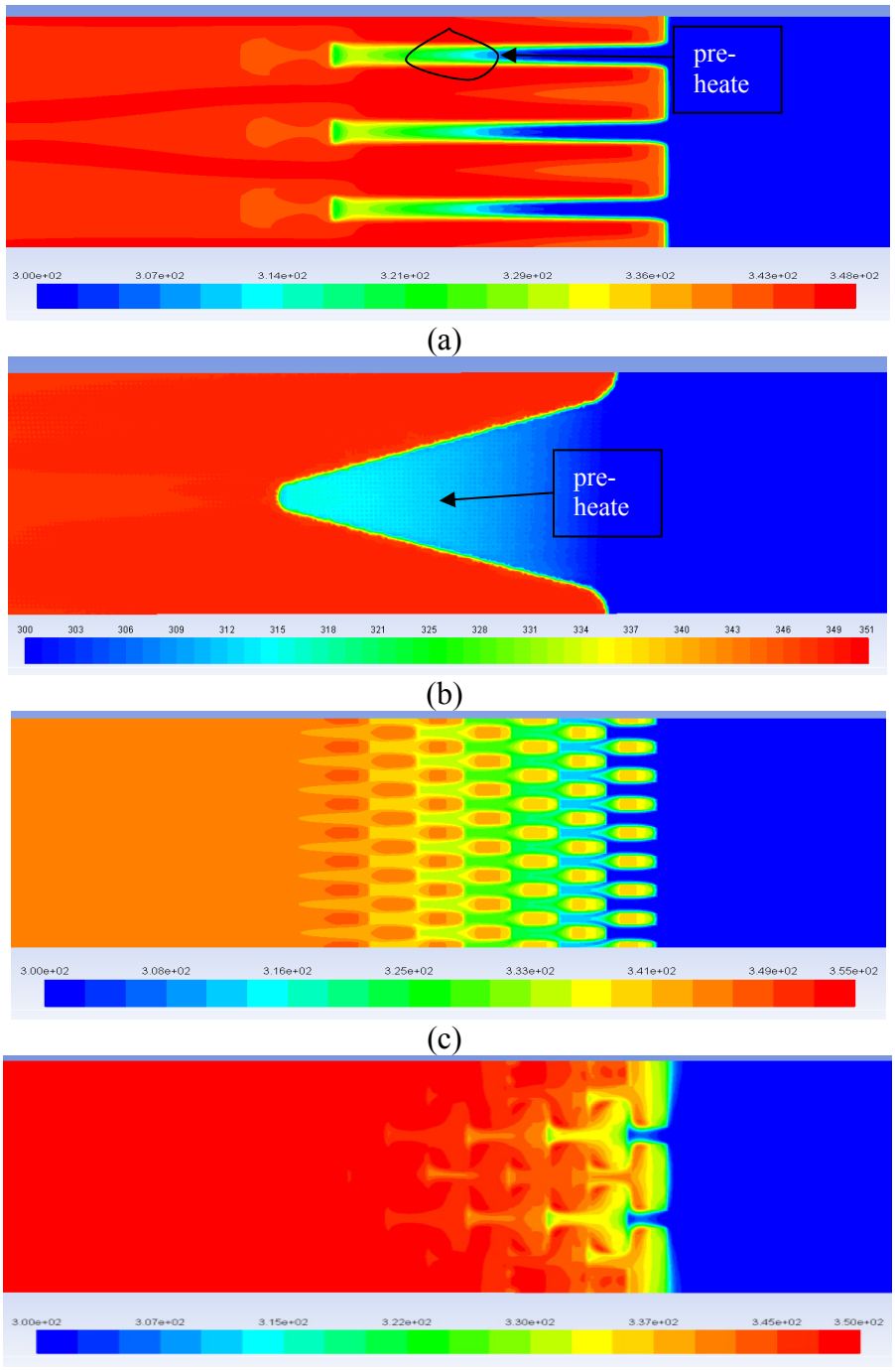

Fig. 4.9. Contours of static temperature (K): (a) corrugated fin; (b) wavy corrugated fin; (c) pin-finned fin; (d) baffle fin.

4.4 Performance comparison between countercurrent flow HEX (made in graphite foam or aluminum) and cross flow aluminum HEX

After the comparison of various configurations of aluminum fins and graphite foam fins, it is found that the louver fin presents higher thermal performance and lower pressure loss than the pin fin and wavy fin in the countercurrent flow HEX; Moreover, the wavy corrugated fin configuration presents better thermal performance and lower flow resistance than the baffle-, pin-finned- and corrugated fins in the graphite foam fin. Thus, the louver fin is chosen as the fin configuration in the aluminum HEX for countercurrent flow condition. Meanwhile, the wavy corrugated fin is adopted as the fin configuration in the graphite foam HEX for countercurrent flow condition.

In order to evaluate the performance of the countercurrent flow HEX, a cross flow aluminum louver fin HEX (the same louver fin as the countercurrent flow HEX) is set as the base. The performance of the graphite foam HEX and aluminum HEX for countercurrent flow condition is investigated by using the ANSYS FLUENT software. The performance of the aluminum HEX for cross flow condition is based on the experimental data from [25].

In order to compare the performance of the countercurrent flow HEX (made in aluminum or graphite foam) and the cross flow HEX (made in aluminum), the heat transfer coefficient is predicted and analyzed. Moreover, the pressure drop is used to analyze the flow characteristics. An overall performance comparison is also carried out to evaluate:

1) Coefficient of performance (COP): defined as how much heat can be dissipated by a certain input pumping power;

$$COP = \frac{Q_{removed}}{P_{pump}} = \frac{Q_{removed}}{u_{in}A_{in}\Delta p} \tag{28}$$

2) Power density (PD): defined as how much heat can be dissipated by a certain mass of fins;

$$PD = \frac{Q_{removed}}{1000 \cdot m_{HEX}} \tag{29}$$

3) Compactness factor (CF): defined as how much heat can be dissipated in a certain volume;

$$CF = \frac{Q_{removed}}{1000 \cdot V_{HEX}} \tag{30}$$

4.4.1 Pressure loss

Because the same louver fins are used on the air side for both the cross flow aluminum HEX and the countercurrent flow aluminum HEX, accordingly, the flow

resistance on the air side is the same for the both cases. Thus, the pressure loss of the cross flow aluminum HEX is not considered here.

The pressure loss through the graphite foam is based on Forchheimer extended Darcy's equation. Fig. 4.10 illuminates that the pressure drop through the graphite foam fin and the aluminum louver fin is a function of the frontal air velocity. The pressure drops increase with increasing frontal velocity. However, the pressure drop through the graphite foam is much higher than that of the aluminum louver fin. Meanwhile, the pressure drop is increased much faster in the graphite foam than in the aluminum louver fin. This means that a high flow resistance appears in the graphite foam. The high flow resistance in the porous graphite foam is associated with many small size pores in the graphite foam. The large internal surface in the graphite foam also increases the hydrodynamic loss.

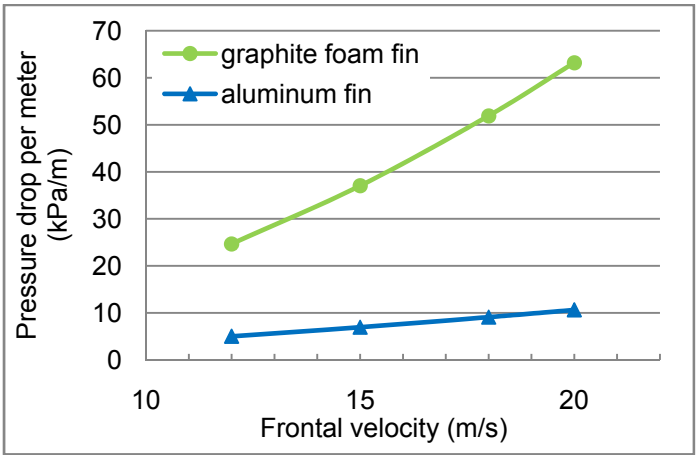

Fig. 4.10. Pressure drops at different velocity.

4.4.2 Thermal performance

The heat transfer coefficient of the cross flow HEX and the countercurrent flow HEX are shown in Fig. 4.11. The heat transfer coefficients increase with increasing frontal velocity. The countercurrent flow HEX presents higher heat transfer coefficient than the cross flow. Because the countercurrent flow arrangement may maximize the temperature difference between two fluids, the countercurrent flow arrangement can transfer more heat than the cross flow arrangement. For the frontal velocity of air in the range of 15 to 20 m/s, the heat transfer coefficient of the countercurrent flow aluminum HEX is 21 % to 9.8 % higher than the one in the cross flow aluminum HEX. The high heat transfer coefficient is beneficial in reducing the size of the countercurrent flow HEX.

Furthermore, the heat transfer coefficients predicted in the graphite foam wavy corrugated fin and the aluminum louver fin (for the countercurrent flow) are also shown in Fig. 4.11. It is found that the heat transfer coefficient in the graphite foam fin increases faster than the one in the aluminum louver fin. The heat transfer coefficient of the graphite foam fin is much higher than that of the aluminum fin. Thus, the thermal performance in the graphite foam fin is high. This is mostly because of the special structure of the graphite foam, in which there are many open pores connected together. Furthermore, the air changes its direction very frequently by the inducement of the foam structure. In this case, the air can be mixed sufficiently in the

graphite foam to increase the heat transfer coefficient. Meanwhile, there is an extremely high thermal conductivity in the graphite foam. The heat transfer inside the solid foam is so efficient that a high temperature difference exists between the air and fin wall. All these factors contribute to the high thermal performance of the graphite foam fin.

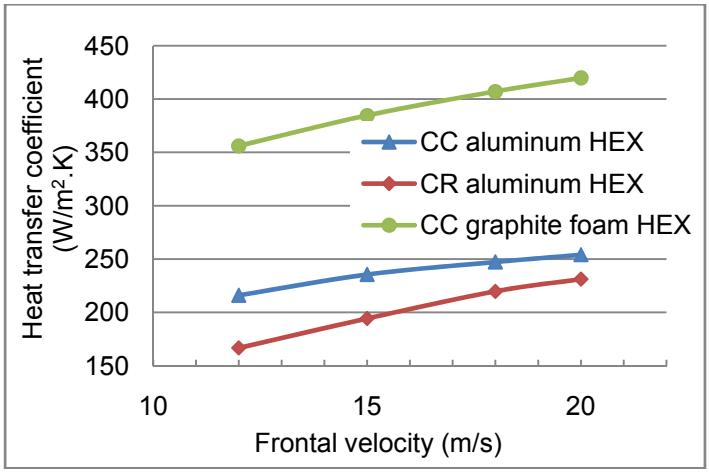

Fig. 4.11. Heat transfer coefficients at different velocity (CC: countercurrent flow; CR: cross flow).

4.4.3 Overall performance

Coefficient of performance (COP)

In order to compare the graphite foam fin with the aluminum louver fin by an appropriate method, the coefficient of performance (COP) is adopted. The simulation results for the COP are shown in Fig. 4.12. The COP values reduce when the velocity is increased. It is noted that the COP value of the countercurrent flow aluminum HEX is higher than that for the cross flow aluminum HEX, because of the high heat transfer coefficient in the countercurrent flow aluminum HEX. However, the COP of the countercurrent flow graphite foam HEX is lower than that of the cross flow aluminum HEX and the countercurrent flow aluminum HEX. This is mostly because of the extremely high flow resistance in the graphite foam, which counteracts the high thermal performance of the graphite foam fin design.

However, the COP of the aluminum HEX is reduced faster than the one in the graphite foam HEX. By increasing the velocity, the difference in COP between the graphite foam HEX and the aluminum HEX is reduced. Based on Fig. 4.12, if the graphite foam HEX should have the same COP value as the aluminum HEX, then the air velocity should be extremely high. Thus, it is difficult to reach the same COP by increasing the velocity.

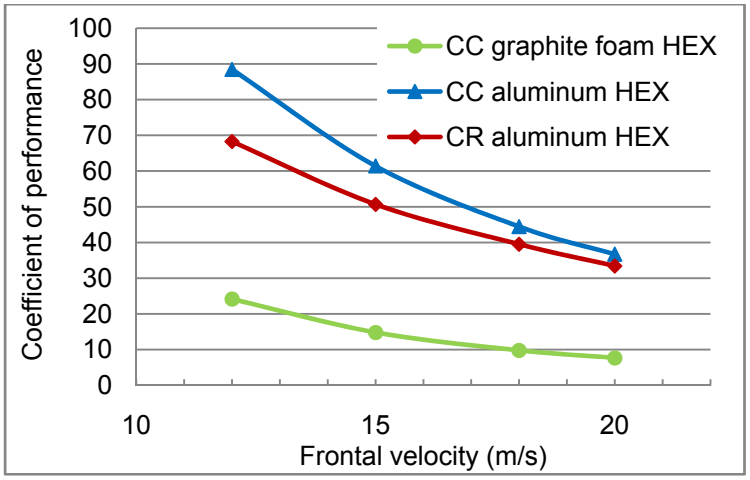

Fig. 4.12. Coefficient of performance in corrugated and pin-finned foams and louver fin.

Power density (PD)

As the power density is considered, it is found that the countercurrent flow graphite foam HEX provides much higher PD value than the countercurrent flow aluminum HEX and the cross flow aluminum HEX, as shown in Fig. 4.13. Moreover, the PD superiority of the countercurrent flow graphite foam HEX becomes more and more evident as the velocity is increased. The higher the PD value is, the lighter the HEX is. Thus, the countercurrent flow graphite foam HEX is much lighter than the countercurrent flow aluminum HEX and the cross flow aluminum HEX, as the dissipated heat is the same. This is mainly attributed to the small density of the graphite foam. The light graphite foam HEX will reduce the weight of the heavy vehicle and save fuel for a vehicle, in which the convectional radiator occupies most of the space and the weight of vehicle.

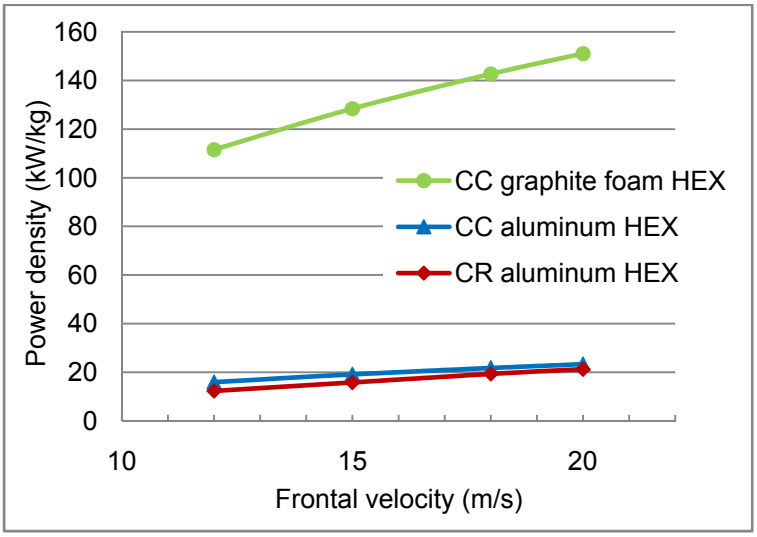

Fig. 4.13. Power density of corrugated and pin-finned foams and louver fin.

Compactness factor (CF)

Fig. 4.14 reveals that the compactness factor (CF) of the countercurrent flow HEX is higher than that of the cross flow HEX. Furthermore, the countercurrent flow graphite foam HEX has higher CF value than the countercurrent flow aluminum HEX. This implies that the volume of the countercurrent flow graphite foam HEX is the smallest one among these three cases, as the dissipated heat is the same. The graphite foam can provide much larger heat transfer surface than the alumnium louver fin HEX, due to many open cells in the graphite foam. Meanwhile, the thermal conductivity of the graphite foam is much higher than that of the aluminum. Thus, the volume of the graphite foam HEX can be reduced significantly. The heat exchanger with high compactness is very favorable in vehicle cooling systems, due to the space limitation in vehicles. Thus, the graphite foam is a potential thermal material for HEXs to reduce the size in vehicles.

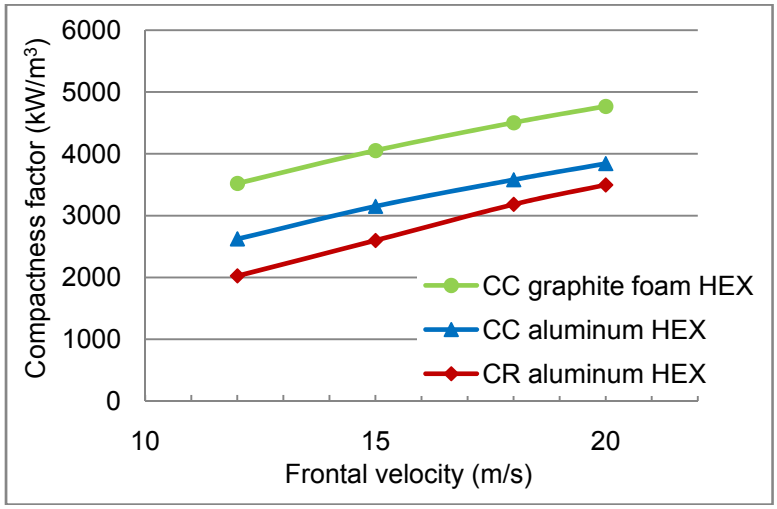

Fig. 4.14. Compactness factor for corrugated and pin-finned foams and louver fin.

4.5 A case study

In order to evaluate the performance of a countercurrent flow HEX and compare it with a cross flow HEX, a typical truck with 400 kW cooling power is considered. The operating data is shown in Table 4.3.

Table 4.3. Assumed operating data of a truck.

Cooling power (kW)	400	
Truck speed (km/h)	65	
Radiator (water side)	T_{in} = 90 °C	T_{out} = 85 °C
Radiator (air side)	T_{in} = 30 °C	T_{out} = 50 °C

Based on the heat transfer coefficients obtained in the present work, the total cooling surface area in the cross flow aluminum HEX is 39.06 m^2. Similarly, the total cooling surface area in the countercurrent flow aluminum HEX is 34.36 m^2, and the one for the countercurrent flow graphite foam HEX is only 20.86 m^2, as shown in Table 4.4.

Meanwhile, due to the low CF value in the countercurrent flow aluminum HEX and the countercurrent flow graphite foam HEX, the volume of these two designs are reduced by 11.8 % and 38.8 %, respectively, compared to the cross flow aluminum HEX. Moreover, because of the low PD value in the countercurrent flow aluminum HEX and the countercurrent flow graphite foam HEX, the weight of these two HEXs are reduced by 12.1 % and 74.5 %, respectively, compared to the cross flow aluminum HEX. However, the power for forcing the air through the countercurrent flow graphite foam HEX is approximately 2.5 times higher than that for the cross flow aluminum HEX. This is mostly because of the high flow resistance in the graphite foam HEX. This is also the main reason blocking the development of the graphite foam HEX.

The height of the countercurrent flow HEX is 600~618 mm, which may destroy the streamlines of the flow field of the heavy vehicle, and cause a huge flow resistance to the vehicle. In order to reduce the flow resistance and optimize the performance of the countercurrent flow HEX, the countercurrent flow HEX (1000*618*70 mm or 1000*600*50 mm) is splitted up into three small countercurrent flow HEXs (the size of each one is: 1000*203*70 mm or 1000*200*50 mm). These three countercurrent flow HEXs are placed in the slanting part of the roof of the vehicle as a staircase to reduce the effect of the flow field on the vehicle, as shown in Fig. 4.15.

Table 4.4. Comparison between the cross flow HEX and the countercurrent flow HEX.

	Cross flow aluminum HEX	Countercurrent flow aluminum HEX	Countercurrent flow graphite foam HEX
Total cooling surface area (m^2)	39.06 (base)	34.36 (-12 %)	20.86 (-46.6 %)
Overall size (W*H*L) (mm*mm*mm)	1000*700*70	1000*618*70	1000*600*50
Total volume (m^3)	0.049 (base)	0.0432 (-11.8 %)	0.03 (-38.8 %)
Weight of fins (kg)	7.9 (base)	6.94 (-12.1 %)	2 (-74.5 %)
Power for pushing air through HEX (W)	8014 (base)	7075 (-11.8 %)	28036 (+250 %)

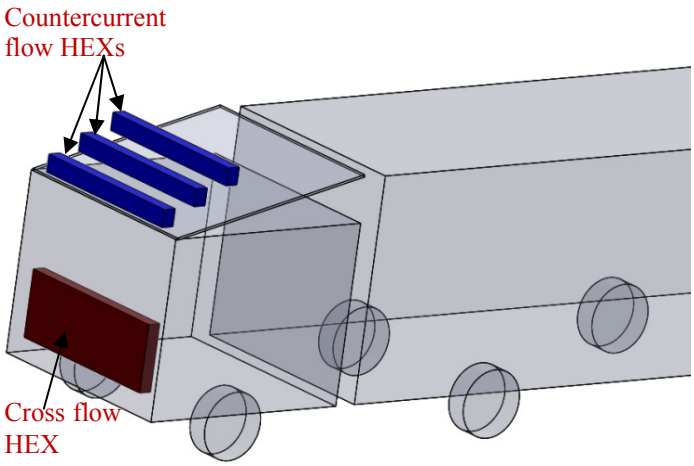

Fig. 4.15. Countercurrent flow HEX and cross flow HEX in a heavy duty truck.

Based on the comparison with the cross flow HEX, the advantages and disadvantages of countercurrent flow HEX can be summarized as follows:

- Advantages:
  (1) The heat transfer coefficient is higher for the countercurrent flow HEX than for the cross flow HEX. Moreover, the graphite foam even further increases the heat transfer coefficient of HEX;
  (2) The overall size of the countercurrent flow HEX is smaller than that of the cross flow HEX, when the dissipated heat is the same;
  (3) The pressure loss will be smaller in the countercurrent flow HEX than in the cross flow HEX, if both are made in aluminum.
  (4) The countercurrent flow HEX has higher PD and CF than the cross flow HEX. This leads to a light and compact HEX in the vehicle.
- Disadvantages:
  (1) The countercurrent flow graphite foam HEX has much higher flow resistance than the cross flow aluminum HEX. Thus, a low COP value is presented for the countercurrent flow graphite foam HEX.
  (2) The countercurrent flow HEX placed on the roof of the vehicle may destroy the streamlines of the flow field around the vehicle. The co-location of the countercurrent flow HEX should be optimized.
  (3) The cooling air through the countercurrent flow HEX is driven by the movement of vehicles. When the vehicle climbs on a mountain, the speed of the vehicle is low. However, the engine cooling power is high at this time. Thus, in future work this problem should be analyzed.

5 Conclusions

Because of the increased cooling requirement in vehicles, an advanced heat exchanger has to be developed for the vehicle industry. However, due to the space limitation in vehicles, placing the heat exchanger at a new place on the vehicles, or using new materials might be favorable in the design of advanced heat exchangers. In this study, a countercurrent flow aluminum HEX is presented for placement on the roof of the driver compartment. Furthermore, due to the high thermal conductivity and low density of graphite foam, a graphite foam HEX is proposed and evaluated under the countercurrent flow condition.

The present work has been carried out by the ANSYS FLUENT software. The simulation models (an aluminum HEX model and a graphite foam HEX model) are validated by experimental results from the literature. A performance comparison between the countercurrent flow HEX (made in aluminum and graphite foam) and the cross flow HEX (made in aluminum) is carried out. The major results are as follows:

1) The louver fin is found to be suitable for the countercurrent flow aluminum HEX, due to better thermal performance and lower pressure drop compared to the wavy fin and the pin fin.

2) The wavy corrugated fin is adopted in the countercurrent flow graphite foam HEX, because of the higher heat transfer coefficient and small pressure loss, compared to the corrugated, pin-finned, and baffle graphite foam fins.

3) When the countercurrent flow HEXs (made in aluminum or graphite foam) are compared with a convectional cross flow aluminum louver fin HEX, the countercurrent flow HEXs provide higher heat transfer coefficient than the cross flow. Especially the one in the countercurrent flow graphite foam HEX provides approximately two times higher heat transfer coefficient than the cross flow aluminum HEX.

4) The power density (PD) and the compactness factor (CF) are much higher for the countercurrent flow HEX than the cross flow aluminum HEX. This implies that the countercurrent flow HEX can be much lighter and compacter than the cross flow HEX.

5) For the specific case given in this study, the total volume of the countercurrent flow aluminum HEX and the graphite foam HEX could be reduced by 11.8 % and 38.8 %, respectively, compared to the cross flow aluminum HEX. Meanwhile, the weight of the fins in the countercurrent flow aluminum HEX and the graphite foam HEX can be reduced by 12.1 % and 74.5 %, respectively, compared to the cross flow aluminum HEX.

Nevertheless, there are still several issues and concerns facing the application of the countercurrent flow HEX in vehicles.

I. Due to the complex internal structure of the graphite foam, the pressure loss in the countercurrent flow graphite foam HEX is much higher than that in the cross flow aluminum louver fin HEX. This leads to a very low coefficient of performance (COP) for the graphite foam HEX. Thus, a large input pumping power is required for the graphite foam HEX. Thus, an appropriate configuration of the graphite foam has to be developed to reduce the pressure drop.

II. The manufacturing methods of graphite foam HEX are not mature, compared to that of aluminum HEX. Furthermore, the mechanical properties of the graphite foam are not as good as those of aluminum.

Thus, much effort has to be spent on the development of countercurrent flow HEXs in vehicles. Especially, much work has to be carried out before graphite foam HEXs appear in the real vehicle cooling systems.

6 Future work

Further investigations to be carried out based on this present work might be:

1) When the position of a HEX in a vehicle is changed, the flow resistance around the vehicle will be different as well. If the new HEX increases the total drag coefficient of the vehicle, then the fuel consumption will be increased. The analysis of the flow field around the vehicle is important as the performance of the vehicle is evaluated. This part of the project work has been carried out by Chalmers University of Technology. Thus, in the future work, co-operative work and data exchange with Chalmers University of Technology should be enhanced. The performance parameters (heat transfer coefficient and pressure drop) of the new HEX will be provided to the research team there. Based on their analysis, the design of the HEX might be modified partly. On the other hand, a parameter analysis of the new HEX will be carried out to optimize the performance of the HEX in future.

2) After comparing the graphite foam HEX with the aluminum HEX, other simulations might be included. Based on a single unit-cube with a spherical void, Yu et al. [31] gave an analytical expression for the effective thermal conductivity of carbon foams. Currently, most of the carbon/graphite foam studies are based on experiments. It is difficult to get the effective thermal conductivity, permeability, and the Forchheimer coefficient theoretically. If the graphite foam structures are reconstructed by building many unit-cubes with spherical voids at a micro scale, then the values of the effective thermal conductivity, permeability, and the Forchheimer coefficient can be obtained, and then the models and simulations can be improved.

3) Another important issue is the manufacturing process for the graphite foam heat exchanger. Muley et al. [50] presented a technology assessment for the metal foam heat exchanger. Several possible manufacturing processes have to be investigated for the graphite foam HEX. Thus, close contacts with heat exchanger industries are needed.

7 References

[1] Davis S. C., Diegel S. W., and Boundy R. G., Transportation Energy Data Book, 29th ed., http://cta.ornl.gov/data/index.shtml.

[2] LaGrandeur J., Crane D., Hung S., Mazar B., and Eder A., 2006, "Automotive waste heat conversion to electric power using Skutterudite, TAGS, PbTe and Bi Te", 2006 International Conference on Thermoelectrics, pp: 343-349.

[3] Johnson V., 2002, "Heat-generated cooling opportunities in vehicles", SAE Technical Paper, No: 2002-01-1969.

[4] Smith K., and Thornton M., 2007, "Feasibility of thermoelectrics for waste heat recovery in hybrid vehicles", http://www.nrel.gov/docs/fy08osti/42256.pdf.

[5] Smith, K., and Wang, C. Y., 2006, "Power and Thermal Characterization of a Lithium-ion Battery Pack for Hybrid-Electric Vehicles", Journal of Power Sources, **160**, pp: 662-673.

[6] 2004, Fuel Cell Handbook. EG&G Technical Services, Inc.

[7] Torregrosa A. J., Broatch A., Olmeda P., and Romero C., 2008, "Assessment of the influence of different cooling system configurations on engine warm-up, emissions and fuel consumption", International Journal of Automotive Technology, **9**(4), pp: 447-458.

[8] Broatch A., Lujan J. M., Ruiz S., and Olmeda P., 2008, "Measurement of hydrocarbon and carbon monoxide emissions during the starting of automotive DI diesel engines", International Journal of Automotive Technology, **9**(2), pp: 129-140.

[9] http://www.answers.com/topic/engine-cooling.

[10] Staunton N., Pickert V., and Maughan R., 2008, "Assessment of advanced thermal management systems for micro-hybrid trucks and heavy duty diesel vehicles", presented at IEEE Vehicle Power and Propulsion Conference (VPPC), Harbin, China, September 3-5, 2008.

[11] Cho H., Jung D., Filipi Z. S., Assanis D. N., Vanderslice J., and Bryzik W., 2007, "Application of controllable electric coolant pump for fuel economy and cooling performance improvement", ASME Journal of Engineering for Gas Turbines and Power, **129**, pp: 239-244.

[12] Li Q., 2004, "Investigation of enhanced heat transfer in nanofluids", Nanjing University of Science & Technology, PhD thesis (in Chinese).

[13] Leong K. Y., Saidur R., Kazi S. N., and Mamun A. H., 2010, "Performance investigation of an automotive car radiator operated with nanofluid-based coolants (nanofluid as a coolant in a radiator)", Applied Thermal Engineering, **30**, pp: 2685-2692.

[14] Kulkarni D. P., Vajjha R. S., Das D. K., and Oliva D., 2008, "Application of aluminum oxide nanofluids in diesel electric generator as jacket water coolant", Applied Thermal Engineering, **28**, pp: 1774-1781.

[15] Al-Hallaj S., Kizilel R., Lateef A., Sabbah R., Farid M., and Selman J. R., 2005, "Passive thermal management using phase change material (PCM) for EV and HEV Li-ion batteries", Vehicle Power and Propulsion, 2005 IEEE Conference, pp: 376-380.

[16] Sabbah R., Kizilel R., Selman J. R., and Al-Hallaj S., 2008, "Active (air-cooled) vs.

passive (phase change material) thermal management of high power Lithium-ion packs: limitation of temperature rise and uniformity of temperature distribution", Journal of Power Sources, **182**, pp: 630-638.

[17] Kizilel, R., Sabbah, R., Selman, J. R., and Al-Hallaj, S., 2009, "An Alternative Cooling System to Enhance the Safety of Li-ion Battery Packs", Journal of Power Sources, **194**, pp: 1105-1112.

[18] Kim K., Choi K., Kim Y., Lee K., and Lee K., 2010, "Feasibility study on a novel cooling technique using a phase change material in an automotive engine", Energy, **35**, pp: 478-484.

[19] Malvicino C., Mattiello F., Seccardini R., and Rostagno M., 2011, "Flat heat exchangers", presented at the Vehicle Thermal Management Systems Conference & Exhibition 10, Warwickshire, UK, May 15-19.

[20] Malvicino C., Sciullo F. D., Cuniberti M., Vestrelli F., and Beltramelli F., 2011, "Dual level vehicle heat rejection system", presented at the Vehicle Thermal Management Systems Conference & Exhibition 10, Warwickshire, UK, May 15-19.

[21] Peuvrier O., Iwasaki M., Hara J., and Mguriya Y., 2011, "Development of compact cooling system (SLIM)", presented at the Vehicle Thermal Management Systems Conference & Exhibition 10, Warwickshire, UK, May 15-19.

[22] Khaled M., Harambat F., Yammine A., and Peerhossaini H., 2010, "Optimization and active control of the underhood cooling system - a numerical analysis", presented at the ASME 2010 3rd Joint US-European Fluids Engineering Summer Meeting and 8th International Conference on Nanochannels, Microchannels, and Minichannels, Montreal (paper No. FEDSM-ICNMM2010-30865), Canada, August 1-5.

[23] Cowell T., and Achaichia N., 1997, "Compact heat exchangers in the automobile industry", presented at Compact Heat Exchangers for the Process Industries, Utah, June 22-27.

[24] Webb R. L., 1995, "Principles of Enhanced Heat Transfer", pp: 3-88, John Wiley & Sons, Inc.

[25] Kays W. M., and London A. L., 1995, "Compact Heat Exchangers", 3rd edition, McGraw Hill Book.

[26] Oliet C., Oliva A., Castro J., and Perez-Segarra C. D., 2007, "Parametric studies on automotive radiators", Applied Thermal Engineering, **27**, pp: 2033-2043.

[27] Carluccio E., Starace G., Ficarella A., and Laforgia D., 2005, "Numerical analysis of a cross-flow compact heat exchanger for vehicle applications", Applied Thermal Engineering, **25**, pp: 1995-2013.

[28] Klett J. W., 2000, "Process for Making Carbon Foam", US Patent 6033506.

[29] Klett J., Hardy R., Romine E., Walls C., and Burchell T., 2000, "High-thermal-conductivity, mescophase-pitch-derived carbon foams: effect of precursor on structure and properties", Carbon, **38**, pp: 953-973.

[30] Klett J. W., Mcmillan A. D., Gallego N. C., and Walls C. A., 2004, "The role of structure on the thermal properties of graphite foams", Journal of Materials Science, **39**, pp: 3659-3676.

[31] Yu Q., Thompson B. E., and Straatman A. G., 2006, "A unit cube-based model for heat transfer and fluid flow in porous carbon foam", ASME Journal of Heat Transfer, **128**, pp: 352-360.

[32] Straatman A. G., Gallego N. C., Thompson B. E., and Hangan H., 2006, "Thermal characterization of porous carbon foam - convection in parallel flow", International

Journal of Heat and Mass Transfer, **49**, pp: 1991-1998.

[33] Paek W. J., Kang H. B., Kim Y. S., and Hyum M. J., 2000, "Effective thermal conductivity and permeability of aluminum foam materials", International Journal of Thermophys, **21** (2), pp: 453-464.

[34] Klett J., Ott, R., and McMillan A., 2000, "Heat exchangers for heavy vehicles utilizing high thermal conductivity graphite foams", SAE Paper 2000-01-2207.

[35] Yu Q., Straatman A. G., and Thompson B. E., 2006, "Carbon-foam finned tubes in air-water heat exchangers", Applied Thermal Engineering, **26**, pp: 131-143.

[36] Garrity P. T., Klausner J. F., and Mei R., 2010, "Performance of aluminum and carbon foams for air side heat transfer augmentation", ASME Journal of Heat Transfer, **132**, 121901-(1-10).

[37] Straatman A. G., Gallego N. C., Yu Q., and Thompson B. E., 2007, "Characterization of porous carbon foam as a material for compact recuperators", ASME Journal of Engineering for Gas Turbines and Power, **129**, pp: 326-330.

[38] Gallego N. G., and Klett J. W., 2003, "Carbon foams for thermal management", Carbon, **41**, pp: 1461-1466.

[39] Leong K. C., Jin L. W., Li H. Y., and Chai J. C., 2008, "Forced convection air cooling in porous graphite foam for thermal management applications", 11th Intersociety Conference on Thermal and Thermomechanical Phenomena in Electronic Systems, pp: 57-64.

[40] Lin Y. R., Du J. H., Wu W., Chow L. C., and Notardonato W., 2010, "Experimental study on heat transfer and pressure drop of recuperative heat exchangers using carbon foam", Journal of Heat Transfer, **132**, 091902-(1-10).

[41] Witry A., Al-Hajer M. H., and Bondok A. A., 2005, "Thermal performance of automotive aluminum plate radiator", Applied Thermal Engineering, **25**, pp. 1207-1218.

[42] Pope S. B., 2000, "Turbulent Flows", Cambridge University.

[43] 2009, "ANSYS FLUENT 12.0 - Theory Guide", ANSYS, Inc..

[44] Tannehill J. C., Anderson D. A., and Pletcher R. H., 1997, "Computational Fluid Mechanics and Heat Transfer", 2nd edition, Taylor & Francis Group LLC.

[45] Yuan J., Huang Y., Sundén B., and Wang W., 2009, "Analysis of parameter effects on chemical reaction couple transport phenomena in SOFC anodes", Heat Mass Transfer, **45**, pp: 471-484.

[46] Lu W., Zhao C. Y. and Tassou S. A., 2006, "Thermal analysis on metal-foam filled heat exchangers. Part I: metal-foam filled pipes", International Journal of Heat and Mass Transfer, **49**, pp: 2751-2761.

[47] Vafai K., 2005, "Handbook of Porous Media", 2nd edition, Taylor & Francis Group LLC..

[48] Versteeg H. K., Malalasekera W., 2007, "An Introduction to Computational Fluid Dynamics", 2nd edition, Pearson Prentice Hall.

[49] Kreith F., 1973, "Principles of Heat Transfer", 3rd edition, Intext Press, Inc.

[50] Muley, A., Kiser, C., Sundén, B., and K Shah, R., 2012, "Foam Heat Exchangers: A Technology Assessment", Heat Transfer Engineering, **33** (1), pp: 42-51.